nature

Accelerated Article Preview

FcγR-mediated SARS-CoV-2 infection of monocytes activates inflammation

Caroline Junqueira, Ângela Crespo, Shahin Ranjbar, Luna B. de Lacerda, Mercedes Lewandrowski, Jacob Ingber, Blair Parry, Sagi Ravid, Sarah Clark, Marie Rose Schrimpf, Felicia Ho, Caroline Beakes, Justin Margolin, Nicole Russell, Kyle Kays, Julie Boucau, Upasana Das Adhikari, Setu M. Vora, Valerie Leger, Lee Gehrke, Lauren Henderson, Erin Janssen, Douglas Kwon, Chris Sander, Jonathan Abraham, Marcia B. Goldberg, Hao Wu, Gautam Mehta, Steven Bell, Anne E. Goldfeld, Michael R. Filbin & Judy Lieberman

This is a PDF file of a peer-reviewed paper that has been accepted for publication. Although unedited, the content has been subjected to preliminary formatting. Nature is providing this early version of the typeset paper as a service to our authors and readers. The text and figures will undergo copyediting and a proof review before the paper is published in its final form. Please note that during the production process errors may be discovered which could affect the content, and all legal disclaimers apply.

Article

FcγR-mediated SARS-CoV-2 infection of monocytes activates inflammation

Caroline Junqueira[1,2,3,16 ✉], Ângela Crespo[1,2,16], Shahin Ranjbar[1,4,16], Luna B. de Lacerda[1,2,3], Mercedes Lewandrowski[1,2], Jacob Ingber[1,2], Blair Parry[5], Sagi Ravid[1,2], Sarah Clark[6], Marie Rose Schrimpf[1,2], Felicia Ho[1,2], Caroline Beakes[5], Justin Margolin[5], Nicole Russell[5], Kyle Kays[5], Julie Boucau[7], Upasana Das Adhikari[7], Setu M. Vora[1,8], Valerie Leger[9], Lee Gehrke[6,9], Lauren Henderson[2,10], Erin Janssen[2,10], Douglas Kwon[7], Chris Sander[11], Jonathan Abraham[6], Marcia B. Goldberg[6,12], Hao Wu[1,2,9], Gautam Mehta[13,14], Steven Bell[15], Anne E. Goldfeld[1,4], Michael R. Filbin[5 ✉] & Judy Lieberman[1,2 ✉]

SARS-CoV-2 can cause acute respiratory distress and death in some patients[1]. Although severe COVID-19 disease is linked to exuberant inflammation, how SARS-CoV-2 triggers inflammation is not understood[2]. Monocytes and macrophages are sentinel cells that sense invasive infection to form inflammasomes that activate caspase-1 and gasdermin D (GSDMD), leading to inflammatory death (pyroptosis) and release of potent inflammatory mediators[3]. Here we show that about 6% of blood monocytes in COVID-19 patients are infected with SARS-CoV-2. Monocyte infection depends on uptake of antibody-opsonized virus by Fcγ receptors. Vaccine recipient plasma does not promote antibody-dependent monocyte infection. SARS-CoV-2 begins to replicate in monocytes, but infection is aborted, and infectious virus is not detected in infected monocyte culture supernatants. Instead, infected cells undergo inflammatory cell death (pyroptosis) mediated by activation of NLRP3 and AIM2 inflammasomes, caspase-1 and GSDMD. Moreover, tissue-resident macrophages, but not infected epithelial and endothelial cells, from COVID-19 lung autopsies have activated inflammasomes. These findings taken together suggest that antibody-mediated SARS-CoV-2 uptake by monocytes/macrophages triggers inflammatory cell death that aborts production of infectious virus but causes systemic inflammation that contributes to COVID-19 pathogenesis.

SARS-CoV-2 causes severe COVID-19 disease marked by acute respiratory distress that can progress to multiorgan failure and death in the elderly and patients with comorbidities[1]. Increased chronic inflammation is associated with aging ("inflammaging") and the comorbidities linked to severe disease[4] and severe disease is linked to signs of inflammation[2]. When myeloid cells sense invasive infection, they activate inflammasomes to sound an innate immune alarm[3]. Inflammasome activation is required to process and release IL-1 family cytokines, arguably the most potent inflammatory mediators[5]. However, activation of NF-κB, the TNF receptor superfamily and T_H17 cytokines can also cause severe inflammation. When inflammasomes sense infection, they recruit the ASC adaptor and assemble into large complexes that recruit and activate caspase-1, which in turn processes interleukin (IL)-1 pro-cytokines and the pore-forming GSDMD to disrupt the cell membrane, leading to cell death and cytokine release[3]. Pyroptotic cell membrane rupture releases cytokines, chemokines and other alarmins that recruit immune cells to infection sites. LDH release is pathognomonic for pyroptosis and other forms of necrotic cell death[3] and elevated LDH is one of the best correlates of severe COVID-19[6].

COVID-19 blood shows signs of pyroptosis

Because inflammasome activation is a major mediator of inflammation[7], we examined SARS-CoV-2-infected patient blood for inflammasome activation and pyroptosis. Freshly isolated mononuclear cells from 19 healthy donors (HD) and 22 COVID-19 patients in the emergency department (ED) were stained for hematopoietic cell markers, a small fixable dye (Zombie Yellow) that enters cells with damaged plasma membranes

and annexin V, an indicator of programmed cell death (Fig. 1a, b, Extended Data Fig. 1a, Supplementary Table 1). Annexin V[+]Zombie^{-} apoptotic cells did not increase in any subpopulation in COVID-19 samples. However, ~6% of monocytes of COVID-19 patients on average took up Zombie dye, a sign of membrane damage consistent with pyroptosis. None of the lymphocyte subsets in COVID-19 samples showed increased pyroptosis. Monocyte flow cytometry indicated a reduced frequency of classical monocytes (CD14^{hi}CD16^{-}) in 15 COVID-19 patients compared to 13 HD, while intermediate monocytes (CD14^{hi}CD16^{+}) were significantly increased, but there was no change in the non-classical subset (CD14^{lo}CD16^{+}) (Fig. 1c, Extended Data Fig. 1b). Many intermediate (~60%) and non-classical (~40%), but none of the more abundant classical, monocytes had taken up SARS-CoV-2 virus since they stained for nucleocapsid (N) (Fig. 1d, e). Since only monocytes that expressed FcγRIIIa (CD16), an important mediator of antibody-dependent phagocytosis, took up virus, anti-spike RBD IgG plasma titers were measured in 64 COVID-19 plasma samples obtained at ED presentation, 20 HD and 5 patients who presented with COVID-19-like symptoms but were SARS-CoV-2 PCR[-] (non-COVID-19 patients) (Fig. 1f). Most COVID-19 patients, but not HD or non-COVID-19 controls, had elevated anti-spike RBD IgG, suggesting that they had been infected for approximately a week[8]. Plasma from COVID-19 patients with diverse disease outcomes and HD were compared for pyroptosis-specific markers (GSDMD, IL-1β, IL-1RA, IL-18, LDH activity) (Fig. 1g), inflammatory markers not specific for pyroptosis (inflammatory cytokines IL-6, TNF, IL-17/17A; growth factors IL-7, G-CSF; chemokines CCL7, CXCL9, CXCL10) and interferons (IFNβ, IFNγ). Consistent with published data[9,10], all inflammation markers not specific for pyroptosis were significantly elevated in COVID-19 plasma (except for IL-17/17A) and IFNs were not detected above baseline (data not shown). All pyroptosis markers were significantly elevated in COVID-19 plasma compared to HD. Although significantly higher in COVID-19 samples, plasma IL-1β, was low, which was not surprising since it is rapidly cleared and usually not detected even in patients with pyroptosis-mediated diseases. However, its antagonist IL-1RA, used as a surrogate[5], was greatly increased in COVID-19 samples. It is worth noting that IL-1 cytokines and pyroptosis potently activate the other elevated inflammation markers[11].

To determine if pyroptosis biomarkers correlate with COVID-19 disease severity, plasma from 10 HD and 60 COVID-19 patients was analyzed for GSDMD, LDH, IL-1RA and IL-18 at presentation and on days 3 and 7 for hospitalized patients (Fig. 1h, Supplementary Table 2). Patients were grouped into mild, moderate or severe disease using the MGH COVID Acuity scale[12]. Plasma GSDMD, LDH, IL-1RA and IL-18 were all elevated in severe samples compared to those with mild or moderate disease, but the increase in GSDMD was not significant. Taken together, these results suggest ongoing pyroptosis in COVID-19 blood that was more prominent in severe disease.

Monocytes have activated inflammasomes

These data suggested that monocytes in COVID-19 patients might die of pyroptosis and release inflammatory cytokines to contribute to poor outcome. Not much is known about how viruses interact with the 27 potential human canonical inflammasome sensors[3]. The NLRP3 inflammasome, which detects K^{+} efflux generated by a variety of stimuli, could be activated by specific viral proteins[13,14]. Three SARS-CoV-2 proteins, Orf3a, Orf8 and the E envelope, are thought to be "viroporins" (ion channels) that potentially activate K^{+} efflux, as previously described for SARS-CoV[15]. Orf3 and Orf8 are only encoded by pathogenic human CoVs. Interestingly, bats, the natural hosts of SARS-CoV and SARS-CoV-2, have a dampened NLRP3 response to multiple viruses, including MERS-CoV, which might explain their toleration of these infections despite high viral loads[16]. To probe whether COVID-19 monocytes undergo pyroptosis, freshly isolated, enriched monocytes from HD, COVID-19 patients of mixed disease severity (Supplementary Table 1) and non-COVID-19

patients were analyzed by imaging flow cytometry for expression and intracellular distribution of the common inflammasome adaptor ASC, activated caspase-1 (by fluorochrome-labeled inhibitor of caspases assay (FLICA)) and GSDMD. Activated canonical inflammasomes form large micron-sized inflammasome-ASC-caspase-1 specks[3]. About 4% of monocytes from COVID-19 patients, 1% of non-COVID-19 patients, but no HD samples, had caspase-1 and ASC specks (Fig. 2a–c; Extended Data Fig. 2a, b). These results suggest that other causes of respiratory distress activate monocyte inflammasomes, but activation is more extensive in SARS-CoV-2 infection. Most cells with ASC specks (~80%) from COVID-19 patients also had co-localized caspase-1 specks (Fig. 2d).

COVID-19 monocytes with ASC specks showed ballooning plasma membranes, GSDMD redistribution from the cytoplasm to cell membrane puncta and Zombie dye uptake, consistent with GSDMD pore formation and pyroptosis, but cells without ASC specks did not (Fig. 2e, f, Extended Data Fig. 2b, e). Most Zombie^{+} cells had ASC specks (62±9%), suggesting that most COVID-19 monocyte death is due to inflammasome activation. However, only 28±5% of cells with ASC specks had taken up Zombie dye. This difference could be because cell membrane permeabilization is delayed after ASC activation and dying cells with damaged membranes are rapidly removed from the blood. Immunoblots of HD and COVID-19 monocyte lysates were probed for full-length GSDMD (GSDMD-FL) and its C-terminal fragment (GSDMD-CT) and housekeeping proteins, β-actin and COX-IV (Fig. 2g, Extended Data Fig. 2g). During pyroptosis, cleaved GSDMD and actin are released and the actin cytoskeleton disintegrates, while membrane-bound proteins, like COX-IV, are mostly retained[3,17]. GSDMD-FL was detected in all HD samples, but in only 1 of 3 COVID-19 samples. GSDMD-CT was detected in COVID-19 monocytes and the positive control (LPS+nigericin-treated HD monocytes). Although COX-IV was detected in all samples, FL β-actin was not detected in one COVID-19 sample, but β-actin fragments were detected in all COVID-19 samples and in nigericin-activated HD monocytes. Thus, COVID-19 monocytes are undergoing pyroptosis.

To identify the activated inflammasome, HD and COVID-19 monocytes were co-stained for ASC and 3 canonical inflammasomes (NLRP3, AIM2 (activated by cytoplasmic DNA) and pyrin (activated by bacterial toxins))[14] (Fig. 2d, h–j, Extended Data Fig. 2c–f). In COVID-19 monocytes, ASC specks co-localized with NLRP3 and AIM2, but there were no pyrin specks. AIM2 activation was unexpected, although AIM2 is activated by RNA viruses in rare cases by an unclear mechanism[18]. AIM2 might sense host mitochondrial DNA since mitochondrial membranes are damaged during pyroptosis[19]. Almost all ASC speck[+] monocytes had co-localized NLRP3 and AIM2 specks (Fig. 2d) and ASC, NLRP3 and AIM2 co-localized (Fig. 2j). We did not expect to find more than one inflammasome stimulated in the same cell, although co-localization of 2 distinct inflammasomes has been reported[20]. Confocal microscopy confirmed ASC, caspase-1, NLRP3 and AIM2 colocalization in inflammasomes selectively in COVID-19 monocytes (Extended Data Fig. 2f). These data showing inflammasome specks and GSDMD membrane localization and cleavage, together with detection of dying Annexin V[-]Zombie[+] monocytes and plasma GSDMD and IL-1 cytokines (Fig. 1), indicate that COVID-19 monocytes die of pyroptosis.

Monocyte infection triggers pyroptosis

But what activates inflammasomes in COVID-19 monocytes? Since inflammasomes sense invasive infection, monocyte infection might be the trigger. A few reports suggest monocytes[10,21] and macrophages can be SARS-CoV-2-infected, and we detected nucleocapsid in patient monocytes (Fig. 1d, e). However, monocytes do not express ACE2, the viral entry receptor[22]. Indeed, ACE2 was undetected or barely detected by flow cytometry and qRT-PCR on COVID-19 and HD monocytes (Extended Data Fig. 3a, b). HD and COVID-19 monocytes expressed similar levels of CD147 (basigin or EMMPRIN), reported to bind to SARS-CoV-2 spike protein and facilitate viral uptake, although this

finding is controversial[23–25] (Extended Data Fig. 3c, d). Monocytes express 3 Fcγ receptors – CD64 (FcγRI) and CD32 (FcγRII), expressed on most blood monocytes, and CD16 (FcγRIIIa), expressed on a small minority of blood monocytes (~10% in HD)[26,27] that are increased in COVID-19[9]. These receptors could recognize antibody-opsonized virions and mediate uptake via antibody-dependent phagocytosis[28]. Anti-SARS-CoV-2 spike antibodies are detected early in SARS-CoV-2 infection, about when patients develop inflammatory symptoms[8,29], as in our cohort (Fig. 1f). To examine whether COVID-19 monocytes are infected, we co-stained HD and COVID-19 monocytes for nucleocapsid (N) (Fig. 3a–d) or dsRNA (J2 antibody) (Fig. 3e–h) and ASC. N staining indicates virus internalization, but J2 staining indicates active infection[30]. HD monocytes did not stain for N, dsRNA or ASC. About 10% of COVID-19 monocytes stained for N or dsRNA (Fig. 3b, f) and ~95% of N+ monocytes were also J2+, indicating viral replication. Virtually all infected cells showed ASC specks (Fig. 3c, g) and all ASC speck+ cells were infected (Fig. 3d, h). Thus SARS-CoV-2 monocyte infection activates inflammasomes and pyroptosis.

Lung macrophages have inflammasome specks

Since the respiratory tract is the main infection site, we next assessed whether macrophages in lung autopsies were infected with SARS-CoV-2 and had active inflammasomes. Fixed lung slides from five human SARS-CoV-2 (Supplementary Table 3) and three uninfected trauma victims were co-stained for CD14, ASC, N and DAPI (Fig 3i–k). In COVID-19 lungs, 15.1±2.9% of CD14- cells and 8.3±4.2% of CD14+ cells stained for N, but N was not detected in trauma victims (Fig 3i–k). As expected, both E-cadherin+ epithelial and CD31+ endothelial CD14- cells stained for N (Fig 3k). However, ASC specks were detected only in CD14+, but not in CD14-, COVID-19 lung cells, indicating that tissue-resident macrophages have activated ASC-containing inflammasomes, but infected lung epithelial and endothelial cells do not. Most CD14+N+ cells had ASC specks (Fig. 3j). ASC specks were not seen in control autopsies. About a quarter of CD14+ lung cells had ASC specks, although only ~8% were N+, suggesting that DAMPs, released from infected or otherwise damaged lung cells, may have activated inflammasomes in uninfected macrophages.

CD16 mediates infection of opsonized virus

To confirm that monocytes can be infected, HD monocytes were infected with an engineered infectious clone (icSARS-CoV-2-mNG) encoding a Neon Green (NG) fluorescent reporter of viral replication[31]. Monocytes, primed or not with LPS, were infected (MOI 1) with reporter virus preincubated with IgG1 isotype control antibody (mAb114), anti-spike mAbs (non-neutralizing C1A-H12, neutralizing C1A-B12)[32] or pooled HD or COVID-19 patient plasma (heat inactivated or not). Antibodies and plasma were also present during culture. After 48 h, monocytes were analyzed for N, dsRNA and ASC by imaging flow cytometry (Fig. 4a–g, Extended Data Fig. 4). Without LPS, anti-spike antibody or COVID-19 pooled plasma, few HD monocytes took up or replicated the virus, but infection increased significantly in the presence of anti-spike mAb or COVID-19 plasma. Antibody neutralizing activity and plasma heat inactivation did not affect infection (Extended Data Fig. 4a–e), suggesting that complement was not involved. IgG-depletion of COVID-19 plasma nearly abrogated viral infection assessed by NG fluorescence, but IgA depletion had no effect on infection (Fig. 4e, j, k). These results suggest infection is mediated by anti-spike antibody-opsonized virus. Nonetheless, N, J2 and NG positive monocytes were detected at low levels after HD monocyte infection with virus preincubated with isotype control mAb or with HD plasma, suggesting possible inefficient anti-SARS-Cov-2 antibody-independent monocyte infection. The highest in vitro infection rate was ~3% in HD monocytes pretreated with LPS and incubated with patient plasma. N and J2 staining were comparable

with low background of ~0.1% in uninfected samples; fewer cells were NG fluorescent (about half as many) and there was no background NG fluorescence. More J2+ or N+ cells in samples with the highest infection rates (treated with LPS and patient plasma or anti-spike antibodies) were also NG fluorescent, indicating viral replication (Extended Data Fig. 4e). NG may be less often detected than N or dsRNA because it is expressed late in the viral lifecycle and/or is more difficult to detect. ASC specks were barely detected in uninfected HD monocytes but increased with SARS-CoV-2 infection (Fig. 4c, Extended Data Fig. 4d). ASC speck+ cells increased when SARS-CoV-2 was preincubated with anti-spike antibody and still more when preincubated with patient plasma. HD monocyte infection with the fluorescent molecular clone was similar to infection with the parental Washington (WA) strain or a Delta variant clinical isolate, but, as expected, the molecular clone less efficiently infected A549-ACE2 than the WA strain or the more infectious Delta variant (Extended Data Fig. 4f, g). The similarity of HD monocyte infection for all three viruses suggested that monocyte viral entry might be ACE2-independent.

To assess whether disease severity or antibodies raised by vaccination increased monocyte virus uptake, LPS-activated monocytes were infected in the presence of pooled plasma from uninfected donors, mRNA vaccine recipients or COVID-19 patients with mild or severe disease. Importantly, uninfected HD and post-vaccination plasma did not facilitate virus uptake or replication, even though plasma anti-RBD IgG was ~2-fold higher in HD vaccine recipients (6.5±1.1 µg/ml) than in COVID-19 patients (3.6±0.5 µg/ml) (Fig. 4f, g). However, non-COVID-19 patient pooled plasma slightly increased infection, but the increase was not significant, suggesting possible inefficient viral uptake by some non-COVID plasma component. Disease severity did not affect infection by COVID-19 patient plasma since pooled mild and/or severe plasma similarly facilitated infection.

Severe acute COVID-19 patients have increased antiviral IgGs that are afucosylated in their Fc region and bind better to CD16[33–35]. To test whether afucosylation affects HD monocyte infection, HD monocyte infection by virus preincubated with purified IgG from pooled HD or COVID-19 plasma or from COVID-19 patients with relatively low (~8%) or high (~30%) afucosylation (2 patients of each) was compared (Fig. 4h, i). As expected, purified HD plasma IgG did not lead to N staining or NG fluorescence, while IgG from pooled COVID-19 plasma did. Low afucosylated IgG did not significantly increase infection compared to HD IgG, but more highly fucosylated COVID-19 IgGs modestly, but significantly, increased N+ cells. However, NG fluorescence did not increase significantly after adding either low or high afucosylated COVID-19 patient IgG, compared to HD IgG, perhaps because this assay is less sensitive than N staining. Purified IgG enhanced HD monocyte infection less than patient plasma (i.e., compare Fig. 4l, m with Fig. 4f, g), suggesting that an Ig-independent plasma component might facilitate infection.

To identify the viral receptor on monocytes, purified HD monocytes were infected with the reporter virus in the presence of COVID-19 patient plasma that was depleted or not of IgG or in the presence of blocking antibodies to potential monocyte receptors - ACE2, CD147 and the three monocyte FcγRs, CD16, CD32 and CD64 (Fig. 4j, k, Extended Data Fig. 5a, b). Blocking CD16 or CD64 or IgG depletion strongly inhibited infection, while blocking the other receptors had no significant effect. The combination of anti-CD16 and anti-CD64 blocking antibody did not inhibit virus uptake more than either blocking antibody on its own. Thus, SARS-CoV-2 infection of monocytes is mostly mediated by CD16 and/or CD64 uptake of opsonized virus.

CD16 is also expressed on neutrophils and cytotoxic T and NK cells, which could be infected by a similar antibody-dependent mechanism. We did not observe increased cell death in patient lymphocytes (Fig. 1a) and therefore didn't study them further. However, neutrophils contribute to SARS-CoV-2 immunopathology and inflammation[36]. To determine whether neutrophils are infected, HD neutrophils and monocytes were infected side by side in the presence of COVID-19 plasma (Extended

Article

Data Fig. 5b, c). Infection of HD neutrophils was low compared to monocyte infection (~0.2% vs almost 3% in monocytes) and not significantly increased above background. To assess whether neutrophils are infected in vivo, the frequency of in vivo neutrophil infection in COVID-19 samples of mixed disease severity and HD was assessed by N staining negatively selected, fresh blood neutrophils (Extended Data Fig. 5d). Infection was not detected in COVID-19 patient neutrophils.

SARS-CoV-2 monocyte infection is aborted

dsRNA and NG detection strongly suggested that monocytes replicate SARS-CoV-2. To confirm viral replication and further assess whether uptake is ACE2-mediated, HD monocytes were infected in the presence of COVID-19 plasma and the antiviral drugs, Remdesivir, an inhibitor of the viral RNA-dependent RNA polymerase, and Camostat mesylate, an inhibitor of TMPRSS2, which primes the spike protein for ACE2-mediated entry[37] (Fig. 4l, m, Extended Data Fig. 5e–g). Monocyte infection, assessed by N or NG positivity, was unaffected by Camostat, but significantly and comparably inhibited by Ig depletion or Remdesivir, confirming antibody-dependent entry and viral replication. Lack of inhibition by Camostat and anti-ACE2 suggests that ACE2 is unlikely to be a dominant receptor for viral entry into monocytes but does not rule out a minor role in monocyte infection or a more prominent role in infection of ACE2+ macrophages. Early in viral replication, a series of +strand subgenomic (sg)RNAs are transcribed with a common leader sequence that specifically indicate viral replication[16]. qRT-PCR was used to detect genomic (g) and sg SARS-CoV-2 RNAs using primers to the N1 region of the N gene and to the shared leader sequence and 3'UTR sequences of the sgRNAs, respectively. gRNA and sgRNA were detected only in SARS-CoV-2-infected HD monocytes (Fig. 4n, o). The most abundant amplified sgRNA fragment migrated on agarose gels at the size of the N sgRNA (1560 nt), and its identity was confirmed by sequencing.

Although multiple assays indicated monocytes begin viral replication, we next assessed whether infected monocytes produce infectious virus. Infectious SARS-CoV-2 is detected in COVID-19 plasma only with especially sensitive assays, and we did not detect infectious virus by plaque assay in 9 COVID-19 plasma samples. Although infected HD monocyte culture supernatants formed plaques in Vero cells when culture supernatants were harvested immediately after infection (likely detecting input virus), no infectious virus was detected when culture supernatants were harvested 48 hours post infection (hpi) (Fig. 4p). By contrast plaques were easily detected in culture supernatants from infected Vero harvested 48 hpi. Thus, monocyte infection did not produce infectious virus.

Discussion

Here we show antibody-opsonized SARS-CoV-2 infects and replicates in blood monocytes and lung macrophages. About 10% of monocytes and 8% of lung macrophages in COVID-19 patients were SARS-CoV-2-infected. We found a one-to-one correspondence between monocyte infection and inflammasome-caspase-1 activation and pyroptosis. Most dying monocytes in COVID-19 blood had activated inflammasomes, suggesting that monocytes are dying of pyroptosis. This is a large number, considering that dying cells are rapidly eliminated in vivo. It may be surprising that monocyte infection and cell death has not been widely recognized. However, this may be because (1) many COVID-19 studies use thawed, frozen cells, and dying cells do not survive freeze-thawing, (2) published studies have not looked at whether circulating mononuclear cells are dying, and (3) few researchers have looked for monocyte infection because monocytes do not express ACE2. A few previous studies have shown increased IL-1 cytokines in COVID-19 plasma, in vitro SARS-CoV-2 entry in myeloid cells or NLRP3 inflammasome-caspase-1 activation in COVID-19 blood cells[9,10,21,38].

However, no previous study showed that SARS-CoV-2 infection of monocytes is antibody-mediated, identified the monocyte receptor, showed that viral replication doesn't produce infectious virions, identified monocyte infection as the cause of inflammasome activation or showed evidence of pyroptosis. However two previous studies suggested that monocyte-derived macrophages (MDM) can be abortively infected[38,39]. In contrast to our findings, MDM weakly express ACE2 and their infection may be partly mediated by ACE2, since in vitro infection in the absence of anti-spike is blocked by anti-ACE2[38,39].

FcγR-mediated uptake of antibody-coated virus into monocytes is a double-edged sword. Pyroptosis, which occurs rapidly, likely aborts viral infection before infectious virions are fully assembled. Monocyte/macrophage infection is a dead end for the virus - it removes virions from the extracellular milieu, blocks them from producing infectious progeny and prevents them from disseminating. Pyroptosis in infected monocytes/macrophages also sounds a potent immune alarm to recruit and activate innate and adaptive immune cells to infection sites to mobilize immune defense. On the other hand, the inflammatory mediators spewed out from pyroptotic monocytes and macrophages can cause cytokine storm. It may not be a coincidence that clinical deterioration coincides temporally with the detection of SARS-CoV-2 antibody responses[8,29,40]. In fact, some recent studies suggest that higher antibody titers correlate with disease severity[29,40].

Pyroptotic myeloid cells are likely a major cause of the serious inflammatory sequelae that lead to acute lung injury, multiorgan damage, vascular leak, and respiratory distress in patients with severe disease. In particular, severe COVID-19 patients had increased plasma biomarkers of pyroptosis compared to mild or moderate patients. However, neither antibody titers nor the proportion of infected ASC speck+ monocytes at presentation correlated with severe disease, perhaps because of the small number of samples. Larger cohorts are needed to better assess the relative importance of monocyte/macrophage pyroptosis in severe COVID-19 pathogenesis. The large numbers of infected monocytes and macrophages, the fact that a quarter of lung macrophages have activated inflammasomes and that myeloid cells are the major source of IL-1 and other inflammatory cytokines make it likely that monocyte/macrophage infection and inflammasome activation are important in severe COVID-19 pathogenesis. Although neutrophils could potentially be infected, infection of freshly isolated COVID-19 neutrophils or in vitro-infected HD neutrophils was not detected. Thus, neutrophil infection is unlikely to be a major contributor to pathogenesis, although neutrophil activation of GSDMD-dependent netosis or other features of neutrophil activation may well be important drivers. It will be worthwhile to study other infected cells as potential sources of inflammation, and to understand what aspects of monocyte/macrophage activation enhance infection.

Four times as many lung-resident macrophages had activated inflammasomes as were infected. Further studies are needed to identify what stimulates inflammation in uninfected macrophages, but alarmins released by lung tissue damage are likely culprits. Although inflammasome activation was detected in virtually every infected monocyte/macrophage, it was not detected in lung epithelial cells. Why lung epithelial cells resist inflammasome activation will require further study. It is worth examining whether infection might activate inflammasome-independent pyroptosis by other gasdermins in non-myeloid cells in the lung. NLRP3 and AIM2 inflammasomes that recognize cell membrane damage and cytosolic DNA, respectively, formed in SARS-CoV-2-infected monocytes. Further work is needed to understand how SARS-CoV-2 activates these inflammasomes, whether activation is restricted to virulent coronaviruses, and whether other inflammasomes are activated, such as NLRP1 and NLRP6, which sense dsRNA[41,42].

In this study blocking antibodies to 2 FcγRs, CD16 and CD64, inhibited monocyte infection. CD64 is expressed on all monocytes, including the dominant classical subtype that are not infected, while CD16 is

more selectively expressed, and all the infected patient monocytes are CD16^{+}. This means that CD16 is likely the major FcR that mediates viral entry into monocytes. Blocking infection by anti-CD64 may be indirect - because CD64 and CD16 use the same signaling adaptors and associate on the cell surface, blocking antibodies to CD64 might interfere with CD16 binding.

At diagnosis, plasma biomarkers of pyroptosis, including IL-1RA, IL-18, LDH and GSDMD, were increased in patients who developed severe disease, suggesting they might help predict prognosis and who would benefit from immune-modulating therapy. Repurposing FDA-approved drugs that inhibit inflammatory cytokines or GSDMD is worth assessing, but so far controlled clinical trials evaluating inhibiting inflammatory cytokines (anti-IL-1β (canakinumab), IL-1RA (anakinra), anti-IL6, anti-IL6R) have shown at best weak protection, which may be due to suboptimal timing or because any cytokine is only one of many inflammatory mediators. Two FDA-approved inhibitors of GSDMD, disulfiram (Antabuse)[43] and dimethyl fumarate (Tecfidera)[44], are currently being evaluated in clinical studies (NCT04485130, NCT04594343, NCT04381936). In mouse models of sepsis, which has overlapping features with severe COVID-19 disease, these drugs strongly improved survival and reduced plasma IL-6 and TNF.

Our findings, which implicate opsonizing antibodies in monocyte infection and inflammasome activation, suggest that antibodies may contribute to deleterious immune reactions associated with severe disease[45]. FcγR-mediated monocyte infection is an example of antibody-mediated enhancement (ADE) of infection. Nonetheless, overwhelming evidence shows that vaccine-generated neutralizing antibodies prevent infection and improve clinical outcome of breakthrough infections, suggesting that anti-spike antibodies are highly beneficial. Plasma from vaccinated individuals did not promote monocyte infection, indicating that ADE is not a concern with respect to vaccination. Therapeutically administered anti-spike neutralizing monoclonal antibodies, however, only improve clinical outcome if given early, before hospitalization[46,47], and antibody-containing convalescent sera have not shown clinical benefit[48]. Thus, it is worth considering whether some antibodies might have both protective and deleterious effects[49]. Antibodies are clearly beneficial for blocking infection of ACE2-expressing lung and airway epithelia, where the virus completes replication to produce infectious progeny. However, antibody properties that affect FcR-mediated cellular uptake, phagocytosis, cytotoxicity and complement activation, can affect disease pathogenesis[28].

Early development of afucosylated anti-spike antibodies promotes alveolar macrophage inflammation and is associated with COVID-19 severity[33–35]. Afucosylated antibodies are increased during acute infection with enveloped viruses like SARS-CoV-2 but are not abundant after COVID-19 vaccination[50] or other types of antigen exposure[34]. IgG isolated from COVID-19 patients with a higher proportion of afucosylated antibodies significantly, but weakly, increased in vitro monocyte infection but IgG from patients with fewer afucosylated antibodies did not. The increased pathogenicity of afucosylated antibodies could be secondary to antibody-mediated infection and downstream inflammasome activation in monocytes and macrophages. However, our findings about afucosylation are preliminary and more work is needed to make this association. Characterizing how antibody features, such as afucosylation, sialylation and choice of constant region, alter protective vs deleterious functions of anti-spike antibodies will be important not only for understanding SARS-CoV-2 pathogenesis, but also for choosing the best preparations of convalescent patient plasma and monoclonal antibodies for therapy and/or prevention of severe disease.

Online content

Any methods, additional references, Nature Research reporting summaries, source data, extended data, supplementary information, acknowledgements, peer review information; details of author contributions and competing interests; and statements of data and code availability are available at https://doi.org/10.1038/s41586-022-04702-4.

1. Hu, B., Guo, H., Zhou, P. & Shi, Z. L. Characteristics of SARS-CoV-2 and COVID-19. *Nat Rev Microbiol,* https://doi.org/10.1038/s41579-020-00459-7 (2020).
2. Del Valle, D. M. et al. An inflammatory cytokine signature predicts COVID-19 severity and survival. *Nat Med* **26**, 1636–1643, https://doi.org/10.1038/s41591-020-1051-9 (2020).
3. Liu, X., Xia, S., Zhang, Z., Wu, H. & Lieberman, J. Channelling inflammation: gasdermins in physiology and disease. *Nat Rev Drug Discov* **20**, 384–405, https://doi.org/10.1038/s41573-021-00154-z (2021).
4. Akbar, A. N. & Gilroy, D. W. Aging immunity may exacerbate COVID-19. *Science* **369**, 256–257, https://doi.org/10.1126/science.abb0762 (2020).
5. Dinarello, C. A. Interleukin-1 in the pathogenesis and treatment of inflammatory diseases. *Blood* **117**, 3720–3732, https://doi.org/10.1182/blood-2010-07-273417 (2011).
6. Wu, C. et al. Risk Factors Associated With Acute Respiratory Distress Syndrome and Death in Patients With Coronavirus Disease 2019 Pneumonia in Wuhan, China. *JAMA Intern Med* **180**, 934–943, https://doi.org/10.1001/jamainternmed.2020.0994 (2020).
7. Vora, S. M., Lieberman, J. & Wu, H. Inflammasome activation at the crux of severe COVID-19. *Nat Rev Immunol* **21**, 694–703, https://doi.org/10.1038/s41577-021-00588-x (2021).
8. Long, Q. X. et al. Antibody responses to SARS-CoV-2 in patients with COVID-19. *Nat Med* **26**, 845–848, https://doi.org/10.1038/s41591-020-0897-1 (2020).
9. Hadjadj, J. et al. Impaired type I interferon activity and inflammatory responses in severe COVID-19 patients. *Science* **369**, 718–724 (2020).
10. Rodrigues, T. S. et al. Inflammasomes are activated in response to SARS-CoV-2 infection and are associated with COVID-19 severity in patients. *J Exp Med* **218**, e20201707, https://doi.org/10.1084/jem.20201707 (2021).
11. Chan, A. H. & Schroder, K. Inflammasome signaling and regulation of interleukin-1 family cytokines. *J Exp Med* **217**, e20190314, https://doi.org/10.1084/jem.20190314 (2020).
12. Filbin, M. R. et al. Longitudinal proteomic analysis of severe COVID-19 reveals survival-associated signatures, tissue-specific cell death, and cell-cell interactions. *Cell Rep Med* **2**, 100287, https://doi.org/10.1016/j.xcrm.2021.100287 (2021).
13. Pan, P. et al. SARS-CoV-2 N protein promotes NLRP3 inflammasome activation to induce hyperinflammation. *Nat Commun* **12**, 4664, https://doi.org/10.1038/s41467-021-25015-6 (2021).
14. Sharma, D. & Kanneganti, T. D. The cell biology of inflammasomes: Mechanisms of inflammasome activation and regulation. *J Cell Biol* **213**, 617–629, https://doi.org/10.1083/jcb.201602089 (2016).
15. Fung, S.-Y., Yuen, K.-S., Ye, Z.-W., Chan, C.-P. & Jin, D.-Y. A tug-of-war between severe acute respiratory syndrome coronavirus 2 and host antiviral defence: lessons from other pathogenic viruses. *Emerging Microbes & Infections* **9**, 558–570 (2020).
16. Irving, A. T., Ahn, M., Goh, G., Anderson, D. E. & Wang, L. F. Lessons from the host defences of bats, a unique viral reservoir. *Nature* **589**, 363–370, https://doi.org/10.1038/s41586-020-03128-0 (2021).
17. Davis, M. A. et al. Calpain drives pyroptotic vimentin cleavage, intermediate filament loss, and cell rupture that mediates immunostimulation. *Proc Natl Acad Sci U S A* **116**, 5061–5070, https://doi.org/10.1073/pnas.1818598116 (2019).
18. Spel, L. & Martinon, F. Detection of viruses by inflammasomes. *Current Opinion in Virology* **46**, 59–64, https://doi.org/10.1016/j.coviro.2020.10.001 (2021).
19. Rogers, C. et al. Gasdermin pores permeabilize mitochondria to augment caspase-3 activation during apoptosis and inflammasome activation. *Nat Commun* **10**, 1689, https://doi.org/10.1038/s41467-019-09397-2 (2019).
20. Swanson, K. V. et al. A noncanonical function of cGAMP in inflammasome priming and activation. *J Exp Med* **214**, 3611–3626, https://doi.org/10.1084/jem.20171749 (2017).
21. Zheng, J. *et al.* SARS-CoV-2-induced immune activation and death of monocyte-derived human macrophages and dendritic cells. *J Infect Dis*, https://doi.org/10.1093/infdis/jiaa753 (2020).
22. Song, X. *et al.* Little to no expression of angiotensin-converting enzyme-2 on most human peripheral blood immune cells but highly expressed on tissue macrophages. *Cytometry A*, https://doi.org/10.1002/cyto.a.24285 (2020).
23. Ragotte, R. J. et al. Human Basigin (CD147) Does Not Directly Interact with SARS-CoV-2 Spike Glycoprotein. *mSphere* **6**, e00647–00621, https://doi.org/10.1128/mSphere.00647-21 (2021).
24. Shilts, J., Crozier, T. W. M., Greenwood, E. J. D., Lehner, P. J. & Wright, G. J. No evidence for basigin/CD147 as a direct SARS-CoV-2 spike binding receptor. *Scientific Reports* **11**, 413, https://doi.org/10.1038/s41598-020-80464-1 (2021).
25. Wang, K. et al. CD147-spike protein is a novel route for SARS-CoV-2 infection to host cells. *Signal Transduct Target Ther* **5**, 283, https://doi.org/10.1038/s41392-020-00426-x (2020).
26. Bruhns, P. & Jonsson, F. Mouse and human FcR effector functions. *Immunol Rev* **268**, 25–51, https://doi.org/10.1111/imr.12350 (2015).
27. Ong, S.-M. et al. A Novel, Five-Marker Alternative to CD16–CD14 Gating to Identify the Three Human Monocyte Subsets. *Frontiers in Immunology* **10**, 1761, https://doi.org/10.3389/fimmu.2019.01761 (2019).
28. Bournazos, S., Gupta, A. & Ravetch, J. V. The role of IgG Fc receptors in antibody-dependent enhancement. *Nat Rev Immunol* **20**, 633–643, https://doi.org/10.1038/s41577-020-00410-0 (2020).
29. Li, K. et al. Dynamic changes in anti-SARS-CoV-2 antibodies during SARS-CoV-2 infection and recovery from COVID-19. *Nat Commun* **11**, 6044, https://doi.org/10.1038/s41467-020-19943-y (2020).
30. Weber, F., Wagner, V., Rasmussen, S. B., Hartmann, R. & Paludan, S. R. Double-stranded RNA is produced by positive-strand RNA viruses and DNA viruses but not in detectable amounts by negative-strand RNA viruses. *J Virol* **80**, 5059–5064, https://doi.org/10.1128/JVI.80.10.5059-5064.2006 (2006).
31. Xie, X. et al. An Infectious cDNA Clone of SARS-CoV-2. *Cell Host Microbe* **27**, 841–848 e843, https://doi.org/10.1016/j.chom.2020.04.004 (2020).

Article

32. Clark, S. A. *et al*. Molecular basis for a germline-biased neutralizing antibody response to SARS-CoV-2. Preprint at *bioRxiv*, https://doi.org/10.1101/2020.11.13.381533 (2020).

33. Chakraborty, S. et al. Proinflammatory IgG Fc structures in patients with severe COVID-19. *Nature Immunology* **22**, 67–73, https://doi.org/10.1038/s41590-020-00828-7 (2021).

34. Larsen, M. D. et al. Afucosylated IgG characterizes enveloped viral responses and correlates with COVID-19 severity. *Science* **371**, eabc8378, https://doi.org/10.1126/science.abc8378 (2021).

35. Hoepel, W. et al. High titers and low fucosylation of early human anti-SARS-CoV-2 IgG promote inflammation by alveolar macrophages. *Sci Transl Med* **13**, eabf8654, https://doi.org/10.1126/scitranslmed.abf8654 (2021).

36. Ackermann, M. et al. Patients with COVID-19: in the dark-NETs of neutrophils. *Cell Death Differ* **28**, 3125–3139, https://doi.org/10.1038/s41418-021-00805-z (2021).

37. Hoffmann, M. et al. SARS-CoV-2 Cell Entry Depends on ACE2 and TMPRSS2 and Is Blocked by a Clinically Proven Protease Inhibitor. *Cell* **181**, 271–280 e278, https://doi.org/10.1016/j.cell.2020.02.052 (2020).

38. Hui, K. P. Y. et al. Tropism, replication competence, and innate immune responses of the coronavirus SARS-CoV-2 in human respiratory tract and conjunctiva: an analysis in ex-vivo and in-vitro cultures. *Lancet Respir Med* **8**, 687–695, https://doi.org/10.1016/S2213-2600(20)30193-4 (2020).

39. Zheng, J. *et al*. SARS-CoV-2-induced immune activation and death of monocyte-derived human macrophages and dendritic cells. *The Journal of Infectious Diseases*, https://doi.org/10.1093/infdis/jiaa753 (2020).

40. Garcia-Beltran, W. F. et al. COVID-19-neutralizing antibodies predict disease severity and survival. *Cell* **184**, 476–488 e411, https://doi.org/10.1016/j.cell.2020.12.015 (2021).

41. Shen, C. et al. Phase separation drives RNA virus-induced activation of the NLRP6 inflammasome. *Cell* **184**, 5759–5774 e5720, https://doi.org/10.1016/j.cell.2021.09.032 (2021).

42. Bauernfried, S., Scherr, M. J., Pichlmair, A., Duderstadt, K. E. & Hornung, V. Human NLRP1 is a sensor for double-stranded RNA. *Science* **371**, eabd0811 (2021).

43. Hu, J. J. et al. FDA-approved disulfiram inhibits pyroptosis by blocking gasdermin D pore formation. *Nat Immunol* **21**, 736–745, https://doi.org/10.1038/s41590-020-0669-6 (2020).

44. Humphries, F. et al. Succination inactivates gasdermin D and blocks pyroptosis. *Science* **369**, 1633–1637, https://doi.org/10.1126/science.abb9818 (2020).

45. Iwasaki, A. & Yang, Y. The potential danger of suboptimal antibody responses in COVID-19. *Nat Rev Immunol* **20**, 339–341, https://doi.org/10.1038/s41577-020-0321-6 (2020).

46. Weinreich, D. M. et al. REGN-COV2, a Neutralizing Antibody Cocktail, in Outpatients with Covid-19. *N Engl J Med* **384**, 238–251, https://doi.org/10.1056/NEJMoa2035002 (2021).

47. Gupta, A. et al. Early Treatment for Covid-19 with SARS-CoV-2 Neutralizing Antibody Sotrovimab. *N Engl J Med* **385**, 1941–1950, https://doi.org/10.1056/NEJMoa2107934 (2021).

48. Korley, F. K. et al. Early Convalescent Plasma for High-Risk Outpatients with Covid-19. *N Engl J Med* **385**, 1951–1960, https://doi.org/10.1056/NEJMoa2103784 (2021).

49. Zhou, Y. et al. Enhancement versus neutralization by SARS-CoV-2 antibodies from a convalescent donor associates with distinct epitopes on the RBD. *Cell Rep* **34**, 108699, https://doi.org/10.1016/j.celrep.2021.108699 (2021).

50. Chakraborty, S. et al. Early non-neutralizing, afucosylated antibody responses are associated with COVID-19 severity. *Sci Transl Med* **14**, eabm7853, https://doi.org/10.1126/scitranslmed.abm7853 (2022).
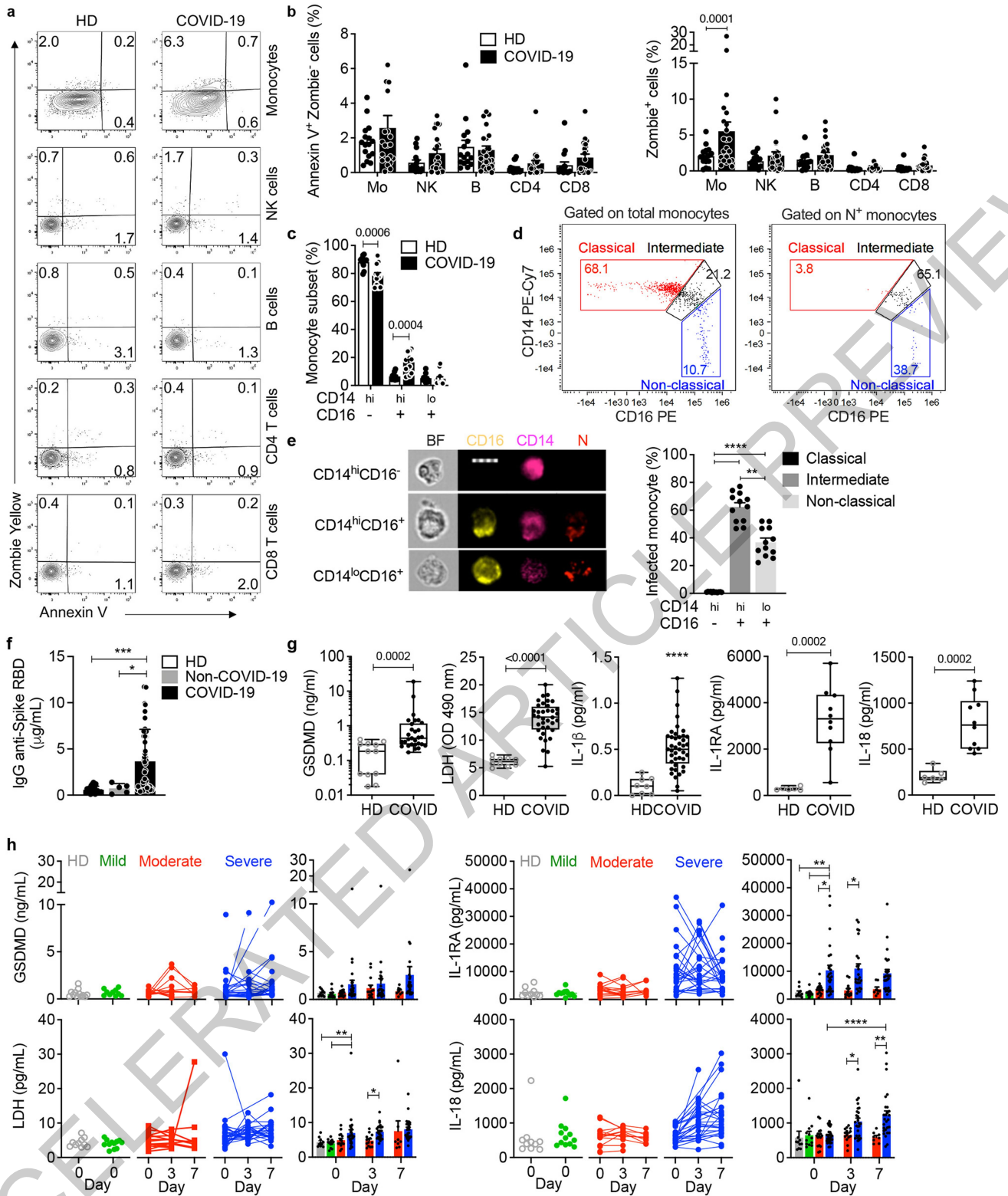
Fig. 1 | See next page for caption.

Fig. 1 | COVID-19 monocytes undergo pyroptosis. a-b, Representative flow cytometry plots (**a**) and percentage of lymphocyte subset and monocyte staining for Annexin V only or Zombie dye (**b**) in fresh blood from HD (n=16) and COVID-19 patients (n=22). **c**, Frequency of monocyte subsets (classical CD14^{hi}CD16$^-$; intermediate CD14^{hi}CD16$^+$; and non-classical CD14^{lo}CD16$^+$) in freshly isolated HD (n=11) and COVID-19 (n=12) blood. **d,e** Imaging flow cytometry of SARS-CoV-2 infection in monocyte subsets of COVID-19 patients (n=12). COVID-19 monocytes were enriched by negative selection and stained for CD14, CD16 and SARS-CoV-2 nucleocapsid (N). Representative dot plots of monocyte subsets gated on all monocytes (left) or N$^+$ monocytes (**d**), representative images of Imaging flow cytometry (left) and quantification of infection (N$^+$) in monocyte subsets (right) (**e**). BF, Brightfield. Scale bar, 7 μm. **f**, Concentration of anti-spike RBD IgG in HD (n=20), non-COVID-19 patients (with COVID-19-like symptoms but PCR- for SARS-CoV-2, n=5) and COVID-19 (n=68) plasma at presentation. **g**, Concentration of pyroptosis biomarkers and cytokines in HD and COVID-19 plasma. GSDMD (HD=12, COVID=29); LDH activity (HD=10, COVID=36); IL-1β (HD=8, COVID=41); IL-1RA and IL-18 (HD=6, COVID=10) (samples described in Supplementary Table 1). **h**, Plasma pyroptosis biomarkers at presentation (day 0) and during hospitalization (day 3 and 7) in COVID-19 patients with mild (n=12), moderate (n=16) and severe (n=32) COVID-19 acuity scores (samples described in Supplementary Table 2). Left panels show individual patient data, right panels, grouped data. Bar graphs show mean ± S.E.M. Box plots with Min/Max Whiskers. *p<0.05, **p<0.01, ***p<0.001, ****p<0.0001 by multiple two-tailed non-parametric unpaired *t*-test (**b,c**), one-way ANOVA with Tukey's multiple comparisons test (**e,f**), two-tailed non-parametric unpaired *t*-test; and two-way ANOVA with Tukey's multiple comparisons test (**h**).
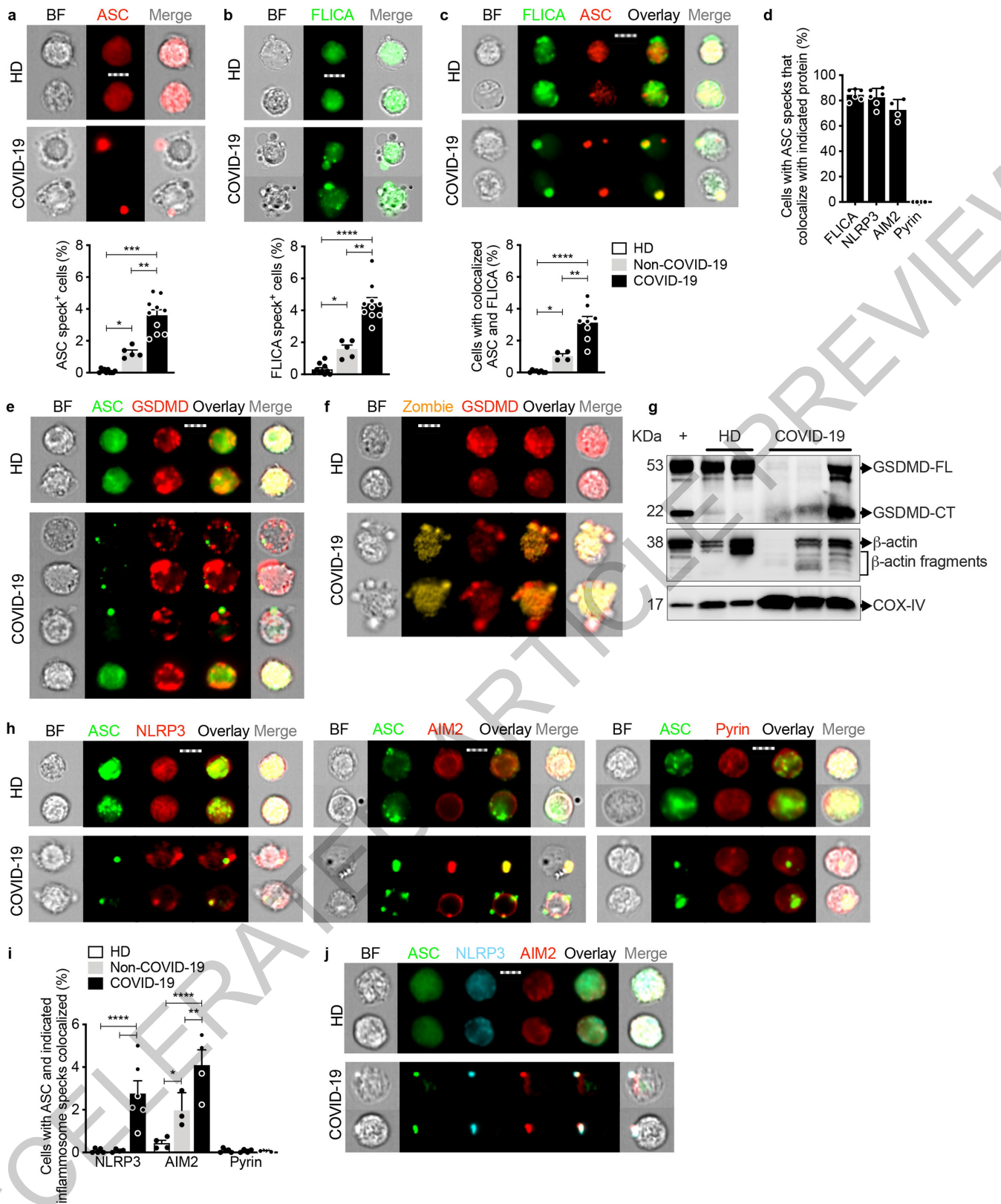
Fig. 2 | See next page for caption.

Fig. 2 | COVID-19 monocytes have activated inflammasomes, caspase-1 and GSDMD. Monocytes from HD, non-COVID-19 or COVID-19 patients at time of presentation were analyzed by imaging flow cytometry for ASC, GSDMD, caspase-1 activation (FLICA) and/or Zombie dye uptake. **a-c**, Percentage of monocytes with activated ASC (**a**) or caspase-1 (**b**) (HD=8, non-COVID=5, COVID=10, **a** and **b**) or colocalized ASC/caspase-1 specks (HD=8, non-COVID=4, COVID=8) (**c**). Representative images are at top and quantification of all samples is at bottom. **d**, Percentage of ASC-speck-containing monocytes with colocalized activated caspase-1, NLRP3, AIM2, or pyrin specks (n=6). **e,f**, Representative images of ASC (**e**) or Zombie dye (**f**) and GSDMD co-stained monocytes (4 independent experiments). **g**, Lysates of purified HD and COVID-19 monocytes and of LPS and nigericin-treated HD monocytes (+) probed with mAb that recognizes full length (GSDMD-FL) and C-terminal (GSDMD-CT) GSDMD (top), β-actin (middle) and COX-IV (bottom); representative of 4 independent experiments. **h,i** Representative images of ASC co-staining with NLRP3 (left, HD=5, non-COVID=4, COVID=6), AIM2 (middle, HD=4, non-COVID=3, COVID=4) and pyrin (right, HD=4, non-COVID=4, COVID=5) (**h**) and quantification of monocytes showing ASC specks colocalized with indicated inflammasomes (**i**). **j**, Representative images of co-staining of ASC, NLRP3, and AIM2 (from 3 independent experiments). Scale bar, 7 μm (**a-c,e,f,h,j**). BF, brightfield. Mean ± S.E.M. is shown. *p<0.05, **p<0.01, ***p<0.001, ****p<0.0001 by one-way ANOVA with Tukey's multiple comparisons test (**a-d**) and by two-way ANOVA with Tukey's multiple comparisons test (**i**).
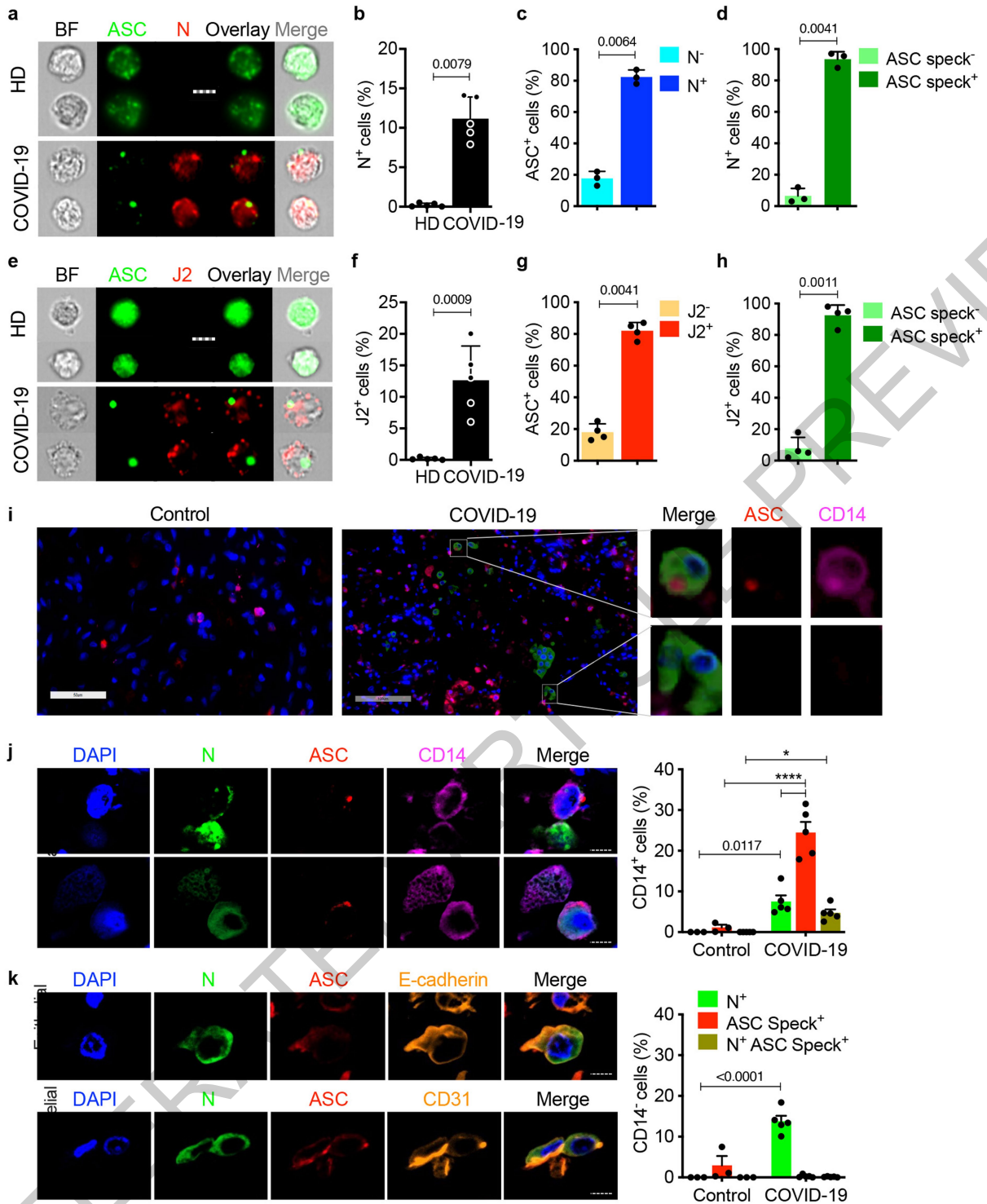
Fig. 3 | SARS-CoV-2-infected monocytes and lung macrophages have activated inflammasomes. a-h, HD and COVID-19 monocytes were stained for SARS-CoV-2 nucleocapsid (N) (n=5) (**a-d**) or dsRNA (J2 antibody) (n=4) (**e-h**) and ASC. Shown are representative imaging flow cytometry images (**a,e**), quantification of infected cells by N (**b**) or J2 (**f**) staining, uninfected or infected cells that showed ASC specks (**c, g**) or percentage of cells with or without ASC specks that were infected (**d,h**). Scale bar, 7 µm (**a,e**). BF, brightfield. **i-k**, Lung autopsies from 5 COVID-19 patients (samples described in Supplementary Table 3) and 3 control trauma victims were stained for N (green), ASC (red), CD14 (magenta) and DAPI (blue). **i**, Digital scanner images of a representative trauma patient (left - Scale bar, 50 µm) and COVID-19 (middle - Scale bar, 100

µm) showing magnified image of representative infected CD14+ (top) and CD14- (bottom) cells from the COVID-19 lung (right). **j,k** (Left) representative confocal microscopy COVID-19 lung images of infected CD14+ (**j**) and CD14- (**k**) cells. (Right) quantification of CD14+ (**j**) and CD14- (**k**) cells that are N+ and/or have ASC specks in COVID-19 (n=5) and control (n=3) lungs. In (**k**), representative images of CD14-N+ cells (left) were co-stained for ASC and E-cadherin, an epithelial marker (top), or CD31, an endothelial marker (bottom). Scale bar, 7 µm (**j,k**). Mean ± S.E.M. is shown. *p<0.05, **p<0.01, ***p<0.001, ****p<0.0001 by two-tailed nonparametric unpaired *t*-test, Mann-Whitney (**b-d,f-h**), and by two-way ANOVA with Tukey's multiple comparisons test (**j,k**).
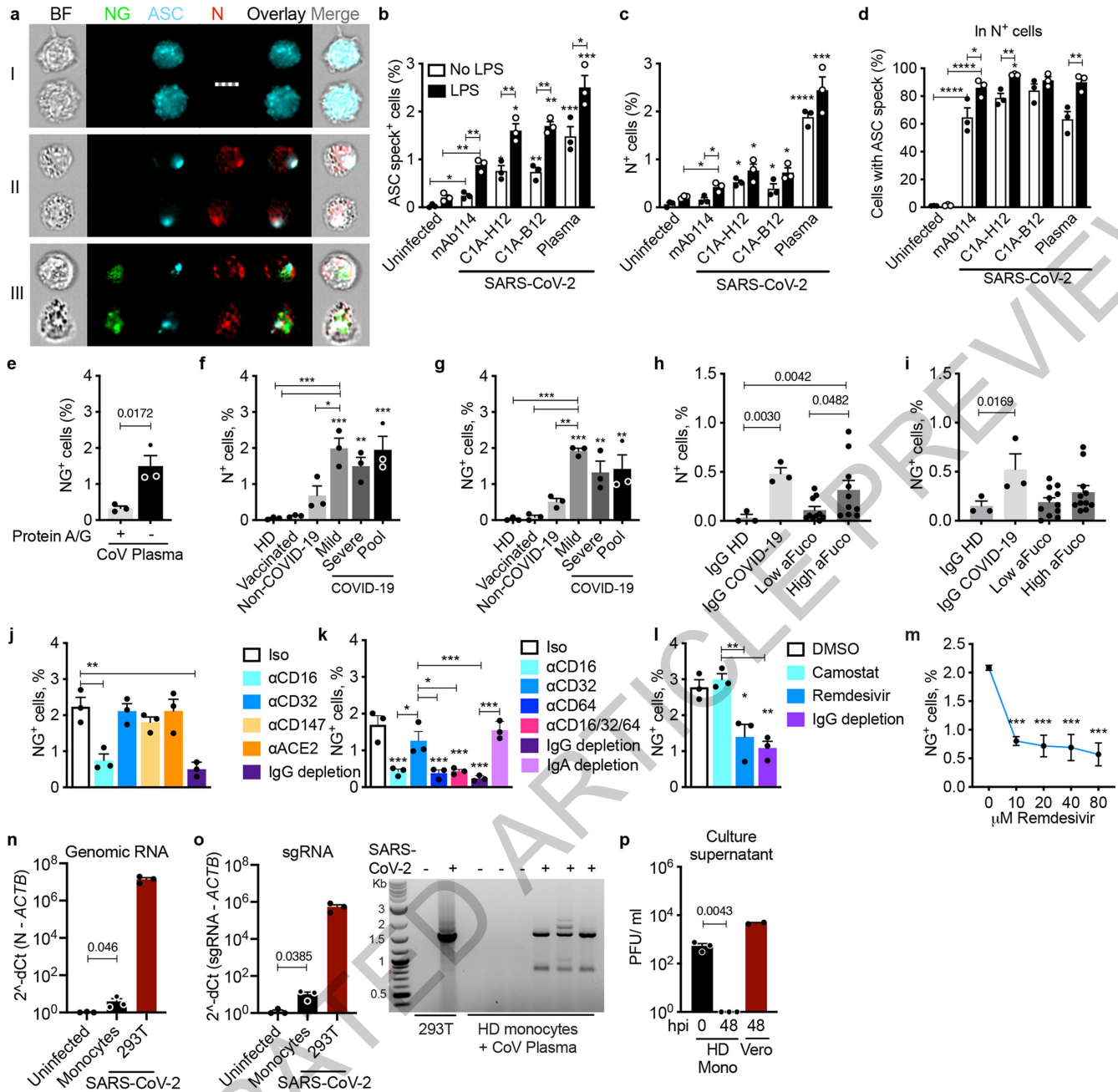
Fig. 4 | HD monocytes take up antibody-opsonized SARS-CoV-2 via an FcγR but viral replication is aborted. a-d, HD monocytes (n=3) were primed (black bars) or not (white bars) with LPS, infected with icSARS-CoV-2-mNG and stained 48 h later for nucleocapsid (N) and ASC. Virus was preincubated with IgG1 control mAb114, non-neutralizing anti-spike (C1A-H12) or neutralizing anti-RBD (C1A-B12) or with pooled COVID-19 plasma, which were present throughout the culture. **a**, Representative imaging flow cytometry images of (I) uninfected (II) N⁺NG⁻ or (III) N⁺NG⁺ monocytes. Quantification of percentage of ASC speck⁺ (**b**) or N⁺ (**c**) monocytes and of N⁺ monocytes with ASC specks (**d**) (n=3). **e-i**, LPS-activated HD monocytes were infected with icSARS-CoV-2-mNG preincubated with pooled COVID-19 plasma, depleted or not of immunoglobulins using Protein A/G beads (n=3, **e**), or preincubated with pooled plasma from HD, COVID-19 mRNA vaccine recipients, or non-COVID-19 patients or COVID-19 patients with mild and/or severe disease (n=3, **f,g**) or with purified IgG from HD (n=3), pooled COVID-19 patients of mixed severity (n=3) or COVID-19 patients with low (~8%) or high (~30%) afucosylated anti-Spike IgG (n=11) (**h,i**). Infection was quantified by N staining (**f,h**) or NG fluorescence

(**e,g,i**). **j-m**, LPS-treated HD monocytes were infected with icSARS-CoV-2-mNG, preincubated with pooled COVID-19 plasma, depleted or not of IgG or IgA as indicated, in the presence of indicated blocking or isotype control (Iso) antibodies (n=3, **j,k**) or antiviral drugs (**l** (10 μM Remdesivir), **m**) and infection was assessed 48 h later by NG fluorescence. Statistics in (**m**) compare drug with no drug. **n,o**, qRT-PCR of genomic SARS-CoV-2 N RNA (**n**) and subgenomic (sg) RNA (**o, left**) in uninfected or infected HD monocytes (n=3), normalized to *ACTB* mRNA. Infected HEK293T were a positive control (n=3). Agarose gel electrophoresis of ethidium bromide-stained qRT-PCR-amplified sgRNA is shown (**o, right**). The ~1600 bp band in the COVID-19 samples was sequenced and confirmed to be *N* sgRNA. **p**, SARS-CoV-2 plaque forming units (PFU) in culture supernatants of infected monocytes (Mono) or Vero E6 harvested at indicated hours post infection (hpi). BF, Brightfield. Scale bar, 7 μm. Mean ± S.E.M is shown. *p<0.05, **p<0.01, ***p<0.001, ****p<0.0001 by two-way ANOVA with Sidak's multiple comparisons test (**b-d**), two-tailed nonparametric unpaired *t*-test (**e**) and one-way ANOVA with Tukey's multiple comparisons test (**f-p**). Data are representative of 3 replicate experiments.

Article

Methods

Human subjects

Fresh PBMCs and plasma cohort. The study was approved by the Investigation Review Boards of Boston Children's Hospital and Massachusetts General Hospital (MGH), and all enrolled patients signed an informed consent. 73 patients 18 years or older with clinical symptoms suggestive of COVID-19 infection were enrolled at the time of presentation to the MGH emergency department (ED) from 7/9/20 to 10/15/21. A 10-ml EDTA blood sample was transported to Boston Children's Hospital and processed within 2 h of collection. COVID-19 samples were all qRT-PCR verified for SARS-CoV-2 infection at the day of blood drawn. Patients who presented to the ED but were PCR- were used as non-COVID-19 samples. Patients who had received SARS-CoV-2 vaccination prior to presentation were excluded from the study. Demographic and clinical data are summarized in Supplementary Table 1. Healthy donor (HD) samples were processed and analyzed in parallel with patient samples. Subjects were enrolled from 7/9/20 to 01/10/21 at Boston Children's Hospital (BCH) with IRB-approved waiver of informed consent. Vaccinated HD (n=6), who received 2 doses of the Pfizer-BioNtech mRNA vaccine, were enrolled 3 weeks after the second dose and their plasma was pooled to evaluate whether it promoted monocyte infection.

Frozen plasma cohort. 60 patients 18 yr or older with clinical symptoms suggestive of COVID-19 infection were enrolled in the MGH ED from 3/15/20 to 4/15/20 with an IRB-approved waiver of informed consent. Enrolled patients had at least one of the following: (i) tachypnea ≥22 breaths per minute, (ii) oxygen saturation ≤92% on room air, (iii) requirement for supplemental oxygen, or (iv) positive-pressure ventilation. A 10-ml EDTA tube was obtained with the initial clinical blood draw in the ED (n=60). Blood was also obtained on days 3 (n=42) and 7 (n=35) if the patient was hospitalized on those dates. Clinical course was followed for 28 d post-enrollment or until hospital discharge if after 28 d. SARS-CoV-2-confirmed patients (by qRT-PCR) were assigned a maximum acuity score (A1-A5) (A1 – died, A2 – required mechanical ventilation, A3 – hospitalized requiring supplemental oxygen, A4 – hospitalized but not requiring supplemental oxygen, A5 – discharged and not requiring hospitalization)[12]. Patients were grouped based on their worst acuity score over 28 d and divided into three groups for comparison (A1 and A2, severe disease; A3, moderate disease; A4 and A5, mild disease). Only 1 patient was in A4; therefore, most mild patients represent those that were discharged immediately from the ED and thus have only a day 0 sample. Demographic and clinical data are summarized for each outcome group (Supplementary Table 2).

Lung tissue specimens. Lung samples from 5 individuals who died from COVID-19 (Supplementary Table 3) and 3 individuals who died from trauma and without lung disease were obtained from MGH. The study was approved by the institutional review board of MGH IRB # 2020P001147. Informed consent was obtained from relatives of study participants. Lung tissue specimens were obtained within 24 h of autopsy and immediately formalin fixed and embedded in paraffin.

Reagents and Antibodies

A listing of reagents and antibodies and their sources is provided in Supplementary Table 4.

Plasma, PBMC, neutrophils and monocyte isolation

Samples were processed using recommended safety precautions in a BSL-2+ facility. Blood tubes were centrifuged at 2000 rpm for 10 min to separate plasma from blood cells. Plasma was collected to a new tube and incubated or not with 1% Triton X-100 for 1 h on ice before aliquoting and freezing at -80 °C. Blood cells were resuspended in PBS and layered over Ficoll for density centrifugation. PBMC were collected from the interface and subjected to red blood cell lysis (if necessary) with Red Blood Cell Lysing Buffer Hybri-Max for 5 min on ice, followed by quenching with RPMI medium supplemented with 10% FBS and 1% Penicillin/Streptomycin. PBMC were washed once more with RPMI and one fraction was stained for flow cytometry, while the remaining cells were used for monocyte purification by negative selection using RosetteSep Human Monocyte Enrichment Cocktail. COVID-19 patient neutrophils were isolated from the whole blood by immunomagnetic negative selection using the EasySep Direct Human Neutrophil Isolation Cocktail, according to the manufacturer's instructions. HD monocytes for in vitro infection were purified from PBMC by positive selection with CD14+ magnetic beads. The red blood cell pellet from the Ficoll density centrifugation was used to isolate neutrophils from the same HD samples. Neutrophils were separated from the RBC pellet by hypotonic lysis.

Cell lines

THP-1 monocytic cell line and Vero E6 cells were obtained from ATCC. A549 and HEK293T cells overexpressing ACE2 cells were obtained from the MassCPR variants repository at Ragon Institute. ACE2 expression was validated by qRT-PCR and anti-ACE2 flow cytometry. All cells were tested for mycoplasma contaminations.

Multiplex Luminex, Immunoassay and LDH activity assay

IL-1RA, IL-2, IL-4, IL-5, IL-6, IL-7, IL-10, IL-12, IL-13, IL-17, IL-18, IL-21, IL-23, CCL3, CCL7, CCL9, CXCL10, G-CSF, TNF, IFN-β and IFN-γ were measured in plasma samples using a custom Luminex assay (R&D Systems), following the manufacturer's instructions. Sample data were aquired using a Luminex xPONENT 4.2 for MAGPIX Analyzer at the Analytical Instrumentation Core Lab of Boston University and analyzed with Milliplex Analyst v5. Plasma levels of IL-1β were measured using Simple Plex cartridge Ella (ProteinSimple), following the manufacturers' instructions at Boston Children's Hospital (BCH). All samples were diluted 1:3 with the dilution buffer and the analytical performance were conducted on the ProteinSimple Ella automated immunoassay platform (Bio-Techne). Samples were aquired Simple Plex Runner 3.7.2.0 software and analyzed with Simple Plex Explorer 3.7.2.0. GSDMD was measured in the same samples using the Human GSDMD ELISA kit (MyBiosource) following the manufacturer's instructions and LDH activity was measured using the CytoTox 96 Non-Radioactive Cytotoxicity Assay (Promega). Results from the latter assays were analyzed using a Biotek Synergy 2 analyzer; GSDMD absorbance was measured at 450 nm and LDH absorbance was measured at 490 nm. Absorbance levels were quantified by linear regression based on the standard curve.

Anti-spike RBD ELISA

Enzyme-linked Immunosorbent Assay (ELISA) kit anti-spike RBD (Bio-Legend) was used to quantify antigen-specific IgG in plasma from HD, non-Covid-19 and COVID-19 patients. ELISA was performed as per manufacturer's instructions. Anti-spike RBD absorbance was measured at 450 nm and 570 nm and quantified by linear regression based on the standard curve.

Intracellular staining for imaging flow cytometry and confocal microscopy

Fixed monocytes were permeabilized with 0.1% Triton X-100 for 10 min and washed twice with PBS + 3% FBS. Monocytes were then blocked for 30 min with PBS + 5% FBS, washed twice and then stained with unconjugated primary antibodies for ASC (1:200, mouse or rabbit), NLRP3 (1:200, goat), AIM2 (1:200, mouse), GSDMD (1:200, mouse), pyrin (1:200, rabbit), dsRNA (J2, mouse) (1:500) or SARS-CoV-2 nucleocapsid protein (1:500, rabbit) for 2 h, followed by 3 washes with PBS + 3% FBS. Cells were then stained with secondary antibodies (donkey anti-mouse, rabbit or goat conjugated with Alexa Fluor 488, 546 or 647, at 1:1000) for 1 h in PBS + 3% FBS, followed by 3 washes. Untreated THP-1 cells, THP-1 treated with LPS + nigericin or transfected with Poly(dA:dT)

using Lipofectamine 2000, and HEK293T cells (negative control) were stained with anti-NLRP3 and anti-AIM2 for antibody validation.

For microscopy, cells were fixed and then stained with DAPI (1:1000) for 10 min, washed 3 times and cytospun onto glass slides (VWR); sealed using polyvinyl alcohol and 1.5 mm coverslips (VWR). Confocal images were acquired using a Zeiss LSM 800 with 405, 488, 561 and 633 nm lasers (emission filters, 465, 509, 561 and 668 nm, respectively) and a 40x or 63x 1.4 oil immersion objective. Images were aquired using Zen Black 2.0 and processed using Zen Blue 3.2.

For imaging flow cytometry, cells were resuspended in PBS + 3% FBS for analysis. Data were acquired using an ImageStream X MKII with 60x magnification (Amnis), acquisition software INSPIRE v2 and analyzed using IDEAS v6.2 software (Amnis). Monocytes were gated based on area/aspect ratio. ASC, NLRP3, AIM2 and pyrin specks were gated and quantified based on fluorophore intensity/max pixels.

Flow cytometry

PBMC were washed and stained for viability with Zombie Yellow in PBS (1:200) for 15 min on ice. Cells were washed with PBS, centrifuged, and then stained with Annexin V PE (1:200) in 1x Annexin Buffer for 15 min on ice. After washing with 1x Annexin V buffer, cells were blocked for 10 min with anti-CD32 (1:100) in PBS + 3% FBS, and then stained for 15 min on ice with a cocktail of antibodies to identify lymphocyte and myeloid cell subsets (all 1:200 except CD19 BV650, CD123 PerCP-Cy5.5 and CD56 APC-Cy7, 1:100). Purified monocytes and an A549 cell line overexpressing ACE2 were blocked with anti-CD32, then stained with primary antibodies for ACE2 (1:100) for 15 min on ice. The secondary anti-goat AF488 was co-incubated with CD14 PE-Cy7 (1:200) and CD147 APC (1:100). After the last wash, cells were resuspended in 2% PFA and kept at 4 °C until flow cytometry analysis. In vitro-infected monocytes were fixed and permeabilized with 0.1% Triton X-100, then blocked with PBS + 5% FBS. Cells were stained with primary antibodies for dsRNA (J2, mouse) (1:500), then stained with secondary antibody (donkey anti-mouse conjugated with Alexa Fluor 647, at 1:500) and anti-CD14 PE-Cy7. Cells were acquired using a FACS Canto II or LSR II with acquisition software FACSDiva v7, and data were analyzed using FlowJo v10.7.1.

FLICA assay

Freshly isolated monocytes were washed and resuspended in RPMI 10% FBS with FLICA substrate (BioRad FAM-FLICA Caspase-1 kit) and cultured for 1 h at 37 °C. Cells were then washed twice with 1X Apoptosis Buffer (from the kit) and fixed with 1x Fixative (from the kit). Cells were kept at 4 °C until further staining and analysis.

Immunoblot

Lysates of enriched monocytes from HD and COVID-19 patients, the former treated or not for 16 h at 37 °C with 100 ng/ml LPS and 20 μM nigericin, were resolved on 12% SDS PAGE gels, transferred to nitrocellulose membranes and blotted to detect GSDMD using (Abcam ab210070) primary rabbit mAb and secondary anti-rabbit IgG. Membranes were also blotted for β-actin and COX-IV.

Immunofluorescence (IF) of lung specimens

Formalin fixed and paraffin embedded lung parenchymal samples were stained for SARS-CoV-2 nucleocapsid (N), ASC, and CD14 and IF was analyzed on the Leica Bond RX automated staining platform using the Leica Biosystems Refine Detection Kit (Leica). The antibody for SARS nucleocapsid (Novus) was run with citrate antigen retrieval and tagged with Alexa Fluor 488 Tyramide (Life). Following citrate stripping, the antibody for CD14 (Cell Signaling) was incubated and tagged with Alexa Fluor 594 Tyramide (Life). Following EDTA stripping, staining for ASC (Santa Cruz) was analyzed using antibody tagged with Alexa Fluor 647 Tyramide (Life). EDTA stripping was performed prior to anti-CD31 or anti-E-cadherin staining tagged to Alexa Fluor 555 Tyramide (Life). Samples were counterstained with DAPI. Slides were scanned using

an Aperio Versa Digital Pathology Scanner (Leica) and analyzed with Aperio ImageScope v12.4.3 software (Leica). Slides were also analyzed by confocal microscopy as described above.

In vitro SARS-CoV-2 infection

icSARS-CoV-2-mNG (a molecular clone of SARS-CoV-2 expressing Neon Green (NG) fluorescent protein) was a gift to AEG from Shi Pei Yong and the World Reference Center for Emerging Viruses and Arboviruses, Department of Microbiology and Immunology, University of Texas Medical Branch, Galveston, TX)[31]. The NG fusion protein is only expressed during viral replication. The SARS CoV-2 US-WA1/2020 ancestral (WA) variant was obtained from BEI Resources. The B.1.617.1 (Delta) variant isolate was obtained from the MassCPR variant repository. In brief, the variant was isolated at the Ragon BSL3 by rescue on Vero-E6 cells from primary clinical specimens. The whole genome of subsequent viral stocks was sequenced to confirm that no additional mutation arose during virus expansion. HD monocytes/neutrophils were purified from apheresis leukoreduction collars collected at Brigham and Women's Hospital. Monocytes were incubated overnight with medium or 100 ng/ml LPS, and then infected with icSARS-CoV-2-mNG, SARS-CoV-2 (WA), and SARS CoV-2 B.1.617.1 (Delta) (MOI =1) in a BSL-3 facility. Infection of A549-ACE2 cells with MOI 0.01 was used as a control. The viral inoculum was treated with 10 μg/ml of antibody (isotype control mAb114, anti-spike C1A-H12, or anti-spike C1A-B12), or 5% HD (n=3), COVID-19 patients of mixed disease severity (n=12, 4 mild, 4 moderate, 4 severe) or vaccinated HD (n=6) pooled plasma (heat inactivated or not; Ig-depleted or not, as indicated) before infection with SARS-CoV-2 for 30 min at room temperature. 100 μl of treated virus was added to monocytes ($2x10^6$ cells/well) in 48 well plates. Infected cells were incubated at 37 °C, 5% CO_2 with gentle shaking every 10 min for 1 h, after which the culture volume was increased to 500 μl with RPMI supplemented with 5% heat inactivated normal AB human serum and 10 μg/ml of the aforementioned antibodies or 5% pooled HD or COVID-19 patient plasma. Cultures were then incubated at 37 °C, 5% CO_2 for 48 h at which time cells were harvested and fixed for 20 min with 4% PFA and then stained.

Immunoglobulin G (IgG) from COVID-19 patient pooled plasma were depleted by protein A/G agarose resin and IgA depleted by Peptide M agarose. Control samples were incubated with agarose resin without coupled protein. C1A-B12 and C1A-H12, two SARS-CoV-2 spike-targeting human monoclonal antibodies, were produced as previously described[32]. For blocking experiments, cells were incubated with 10 μg/ml monoclonal antibodies, α-CD16, α-CD32 (Clone IV.3 - Fig. 4j and Extended Data Fig. 5a; Clone 6C4 - Fig. 4k and Extended Data Fig. 5b, c), α-CD64, α-ACE2, and α-CD147 for 30 min, before virus infection. For antiviral drug treatment, monocytes were incubated at 37 °C, 5% CO_2 for 1 h with 10 μM Remdesivir (GS-5734) or Camostat mesylate prior to infection. To find an appropriate Remdesivir concentration, serial dilutions between 10 and 80 μM were analyzed. To compare plasma obtained from patients with different disease severity, plasma was pooled based on the MGH acuity score (A1-A5), as described above.

To test the role of IgG afucosylation, IgG purified from COVID-19 patient serum samples, was analyzed by mass spectrometry to define the percentage of afucosylation as described[33]. Low afucosylated samples, kindly provided by Prof. Taia Wang (Stanford University), contained 8.4±0□7% afucosylated IgG and high afucosylated samples, 30.1±1.5% afucosylated IgG. IgG was also purified from HD and COVID-19 patient pooled plasma using the Melon gel IgG spin purification Kit (Thermo Fisher Scientific) according to the manufacturer's instructions. Virus was preincubated with 10 μg/ml of purified IgG and the infection was performed as described above.

qRT-PCR

RNA was extracted using Trizol reagent (Invitrogen) from COVID-19 patient monocytes or from uninfected or infected HD monocytes

Article

(stimulated or not with LPS (100 ng/ml for 16 h)), then reverse transcribed using a High-Capacity cDNA Reverse Transcription Kit (Applied Biosystems). Random primers were used to generate cDNA for detection of cellular RNAs (*ACE2*, *BSG*, *ACTB*) and SARS-CoV-2 specific primers were used to generate cDNA to detect viral genomic RNAs (N1 region of *N* gene)[51]. cDNA was analyzed by qRT-PCR using the Sso Fast EvaGreen Supermix (BioRad) (30 sec at 95 °C, 40 cycles (3 sec at 95 °C; 3 sec at 54 °C) in a CFX96 Touch Real-Time PCR Detection System (BioRad) with CFX Manager Software v1.6 acquisition/analysis software. To detect SARS-CoV-2 subgenomic RNA, qRT-PCR was carried out using a primer pair with the forward primer annealing to the 5' leader region of the viral genome and the reverse primer annealing to the 3' UTR. With the cycling conditions used (30 sec at 95 °C, 40 cycles (30 sec at 95 °C, 30 sec at 60 °C, 90 sec at 72 °C)), full-length genomic RNA was not amplified, but small subgenomic RNA segments (<3 kB) could be amplified[16,52,53]. For each sample, Ct values were normalized to the *ACTB* Ct value. Primer sequences are given in Supplementary Table 4. Subgenomic RNA qPCR products were also analyzed by electrophoresis on 1% agarose gels stained with ethidium bromide and visualized on a Chemidoc imager (BioRad). The ~1600 nt band was excised and sequenced to confirm its origin as the SARS-CoV-2 subgenomic RNA encoding for N.

Plaque assays

Vero E6 cells were seeded as monolayers in 24-well plates 1 d prior to infection. Virus-infected sample culture supernatants were serially diluted in DMEM. The plates were washed once with DPBS and then infected with 100 μl of diluted sample and incubated at 37 °C, 5% CO_2 for 1 h with rocking every 15 min. After 1 h, the inoculum was removed and an overlay of 1% methylcellulose (Sigma) in complete MEM (Gibco) was applied to each well. The plates were incubated at 37 °C until plaques were observable in positive control wells. To visualize plaques, the overlay was removed, and the cell monolayer was fixed with 4% PFA and stained with crystal violet. Plaques were then counted to quantify the virus titer in PFU/ml.

Statistical Analysis

Statistical analysis was performed using GraphPad Prism v9.0. Normal distribution of the data was evaluated by the D'Agostino and Pearson normality test prior to applying statistical methods. Distributions were considered normal if $P \leq 0.05$. Parametric or non-parametric (Mann-Whitney test) two-tailed unpaired *t*-tests were used to compare two unpaired groups. Multiple group comparisons were analyzed by one-way ANOVA with Sidak's or Tukey's multiple comparisons tests, or non-parametric Kruskal-Wallis with Dunn's post-test. Multiple groups were compared by two-way ANOVA with additional Sidak's or Tukey's multiple comparisons test. Mean plasma values from hospitalized COVID-19 patients on each day were compared between severity groups by multiple unpaired *t*-tests. Correlations of plasma levels

were determined by simple linear regression and Pearson correlation coefficient.

Reporting summary

Further information on research design is available in the Nature Research Reporting Summary linked to this paper.

Data availability

The data and materials that support the findings of this study are available from the corresponding authors upon request.

51. CDC. 2019-Novel Coronavirus (2019-nCoV) Real-Time rRT-PCR Panel Primer and Probes. https://www.cdc.gov/coronavirus/2019-ncov/lab/rt-pcr-panel-primer-probes.html (2020).
52. Kim, D. et al. The Architecture of SARS-CoV-2 Transcriptome. *Cell* **181**, 914–921 e910, https://doi.org/10.1016/j.cell.2020.04.011 (2020).
53. Perera, R. et al. SARS-CoV-2 Virus Culture and Subgenomic RNA for Respiratory Specimens from Patients with Mild Coronavirus Disease. *Emerg Infect Dis* **26**, 2701–2704, https://doi.org/10.3201/eid2611.203219 (2020).

Extended Data Fig. 1 | Identification of lymphocyte and monocyte subsets in healthy donors and COVID-19 patients. Flow cytometry gating strategy for identifying lymphocytes and monocytes in Fig. 1a, b (**a**) and for identifying monocyte subpopulations in Fig. 1c (**b**). Monocyte subpopulations: CL - classical CD14^{hi}CD16$^-$; ITM - intermediate CD14^{hi}CD16$^+$; NCL - non-classical CD14^{lo}CD16$^+$.
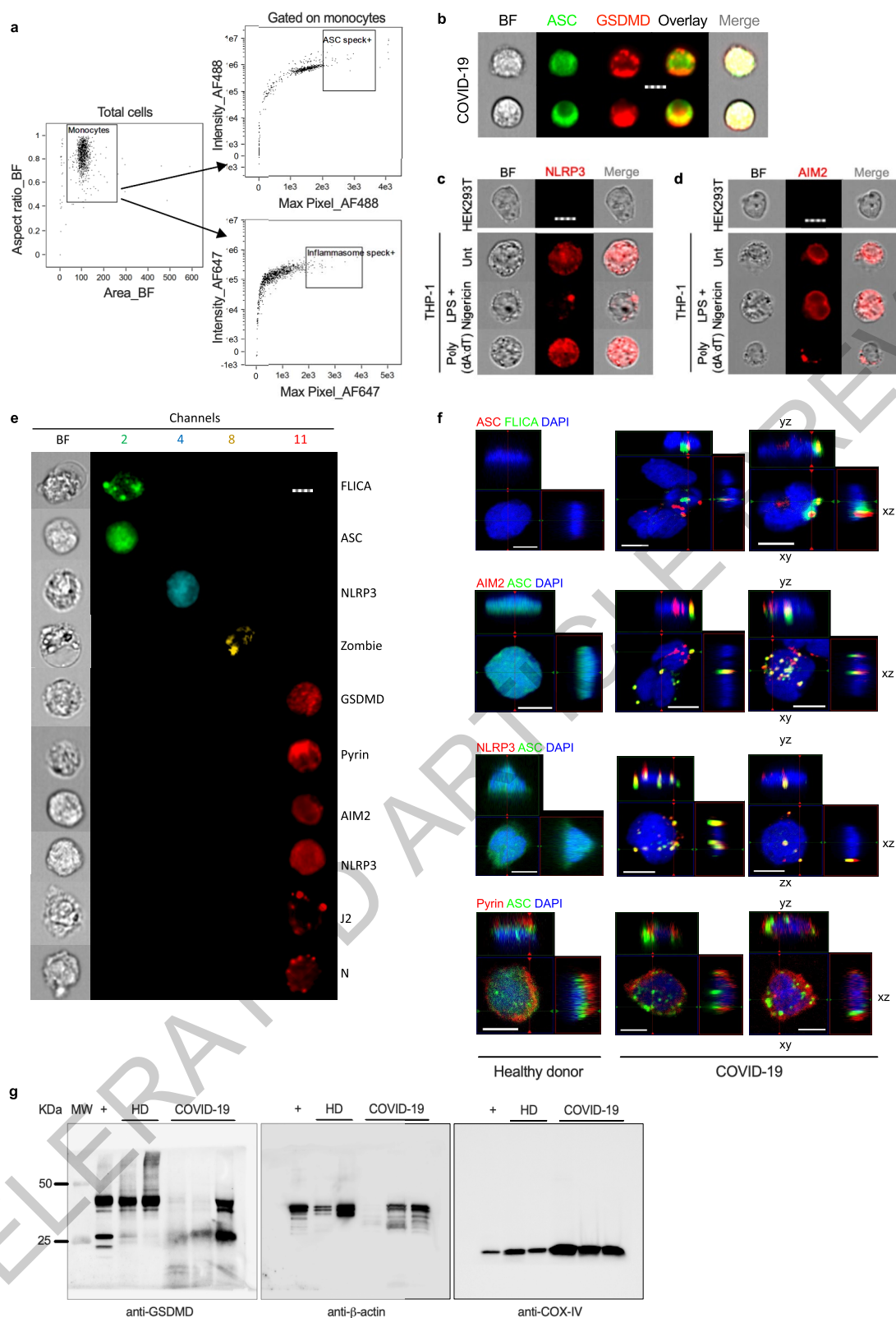
Extended Data Fig. 2 | Inflammasome imaging and GSDMD cleavage analysis. a, Gating strategy for imaging flow cytometry analysis of isolated monocytes. **b**, Representative imaging flow cytometry images of GSDMD and ASC staining in COVID-19 patient monocytes that lacked ASC specks. **c,d**, Representative imaging flow cytometry images of HEK293T cells (negative control) and THP-1 cells untreated or treated with LPS+nigericin or transfected with poly(dA:dT), then stained with anti-NLRP3 (**c**) and anti-AIM2 (**d**). **e**, Single staining controls for antibody staining. Representative images of monocytes

from COVID-19 patients shown were stained with 1° ASC - 2° AF488; 1° NLRP3 - 2° AF568; 1° GSDMD, Pyrin, AIM2, J2, N - 2° AF647; or FAM FLICA Caspase-1 fluorescence, and Zombie Yellow dye. FLICA+ and Zombie+ cells in cells undergoing pyroptosis; GSDMD, Pyrin, AIM2 and NLRP3 in non-pyroptotic cells (diffuse staining); J2+ and N+ in infected monocytes. Scale bar, 7 µm (**b-e**). **f**, Representative confocal image z-stacks and plane projections of monocytes of HD and COVID-19 patients, stained for the same markers as in Figure 2. Scale bars, 5 µm. **g**, Full scan images for blots shown in Fig. 2g.
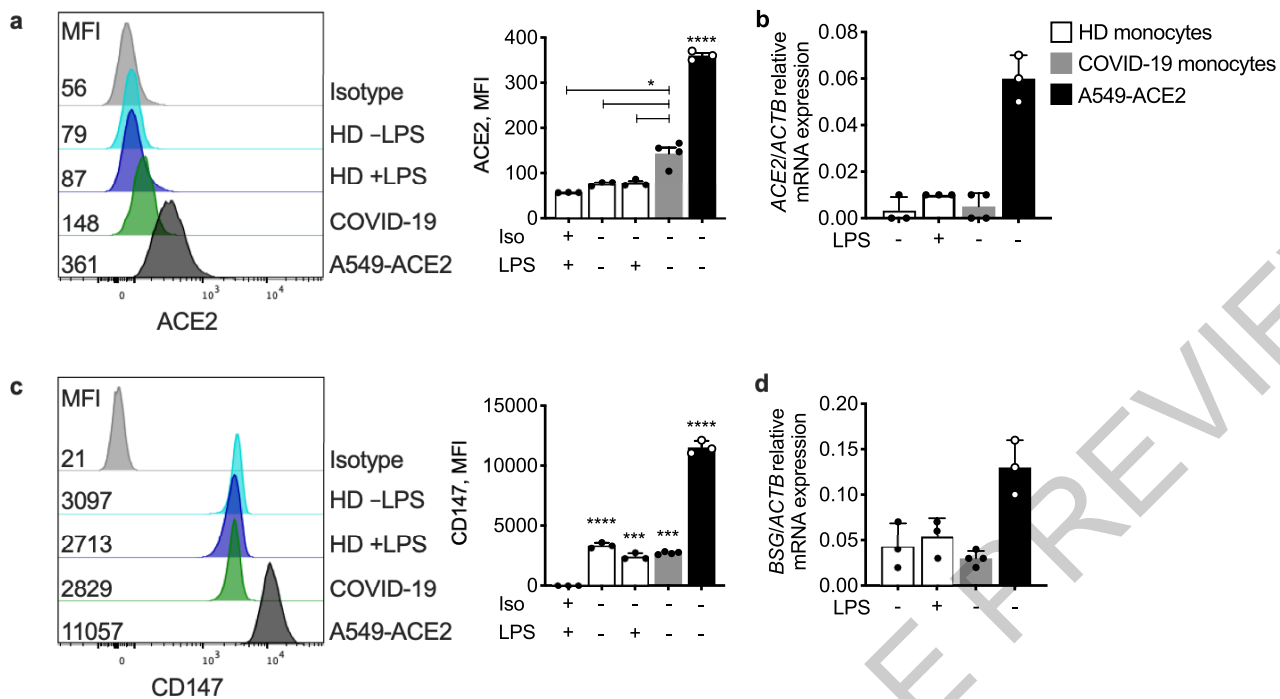
Extended Data Fig. 3 | ACE2 and CD147 expression on circulating monocytes. Purified blood monocytes from HD (n=3), COVID-19 patients (n=4) and A549-ACE2 (n=3) were analyzed by flow cytometry (**a,c**) and qRT-PCR (**b,d**) for expression of ACE2 (**a,b**) or CD147 (*BSG*) (**c,d**). HD monocytes were treated or not with LPS before analysis. A549-ACE2 cells were used as positive control.

Mean ± S.E.M. is shown. *p<0.05, ***p<0.001, ****p<0.0001 relative to isotype (Iso) control antibody-stained, LPS-activated HD monocytes (**a,c**) by one-way ANOVA with Tukey's multiple comparisons test. Data are representative of 2 independent experiments.
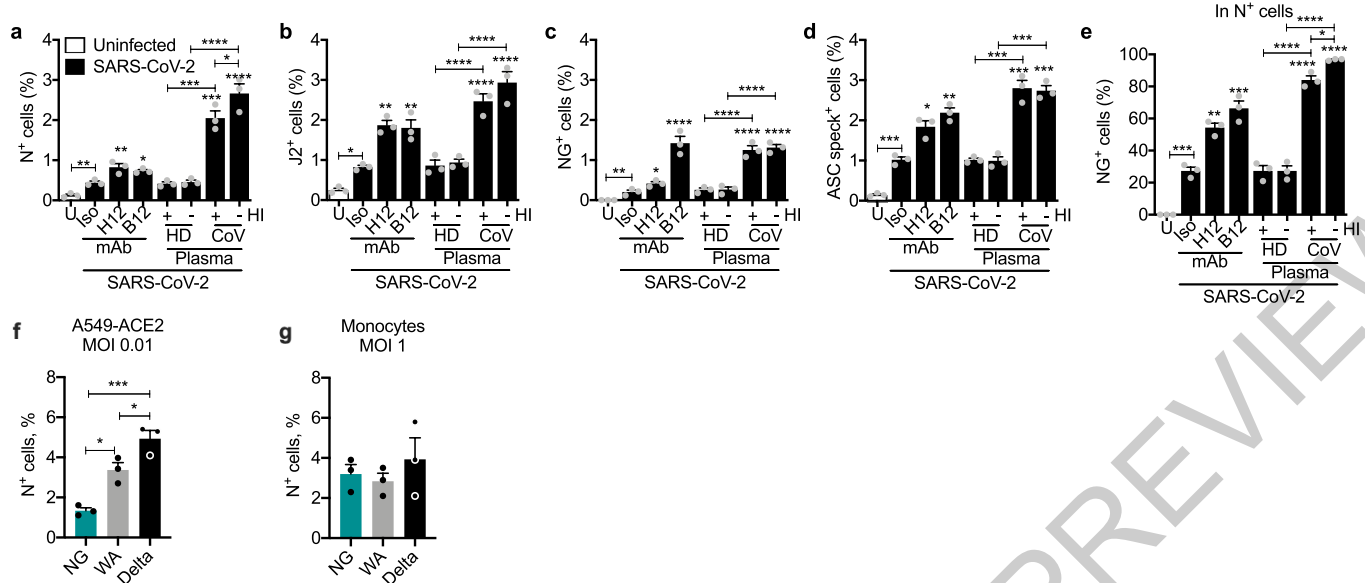
Extended Data Fig. 4 | Effect of anti-spike monoclonal antibodies or pooled COVID-19 plasma on in vitro infection of healthy donor purified monocytes with icSARS-CoV-2-mNG. a-e, HD monocytes (n=3) were primed with LPS, infected with icSARS-CoV-2-mNG (MOI, 1), then stained 48 h later for nucleocapsid (N) or dsRNA (J2) and ASC and analyzed by imaging flow cytometry. Before infection, virus was preincubated with indicated monoclonal antibodies (IgG1 isotype control mAb114 (Iso)), non-neutralizing anti-spike (C1A-H12 (H12)) or neutralizing anti-RBD (C1A-B12 (B12)) or with pooled HD or COVID-19 patient plasma that had been heat-inactivated (HI) or not. U, uninfected. Quantification of HD monocyte staining for N (**a**), J2 (**b**), NG (**c,e**) or ASC specks (**d**). (**e**) Shows the percentage of N+ cells that were also NG fluorescent. **f,g**, A5490-ACE2 (n=3) (**f**) or LPS-primed HD monocytes (n=3) (**g**) were infected at the indicated MOI with icSARS-CoV-2-mNG (NG), a molecular clone of the Washington (WA) strain, or with clinical WA and Delta strains. Infection was measured by N staining and flow cytometry. Mean ± S.E.M. is shown. *p<0.05, **p<0.01, ***p<0.001, ****p<0.0001 by one-way ANOVA with Tukey's multiple comparisons test, relative to Iso or as indicated (**a-g**). Data are representative of 2 independent experiments.

a Monocytes MOI 1

b Monocytes MOI 1

c Neutrophils MOI 1 / Neutrophils MOI 1

d Neutrophils freshly isolated

e Monocytes MOI 1

f A549-ACE2 MOI 0.01

g Monocytes MOI 1 / A549-ACE2 MOI 0.01

Legends:
- Iso
- CD16
- CD32
- CD147
- ACE2
- IgG depletion
- Uninfected
- αCD16
- αCD32
- αCD64
- αCD16/32/64
- IgG depletion
- IgA depletion
- DMSO
- Camostat
- Remdesivir
- IgG depletion
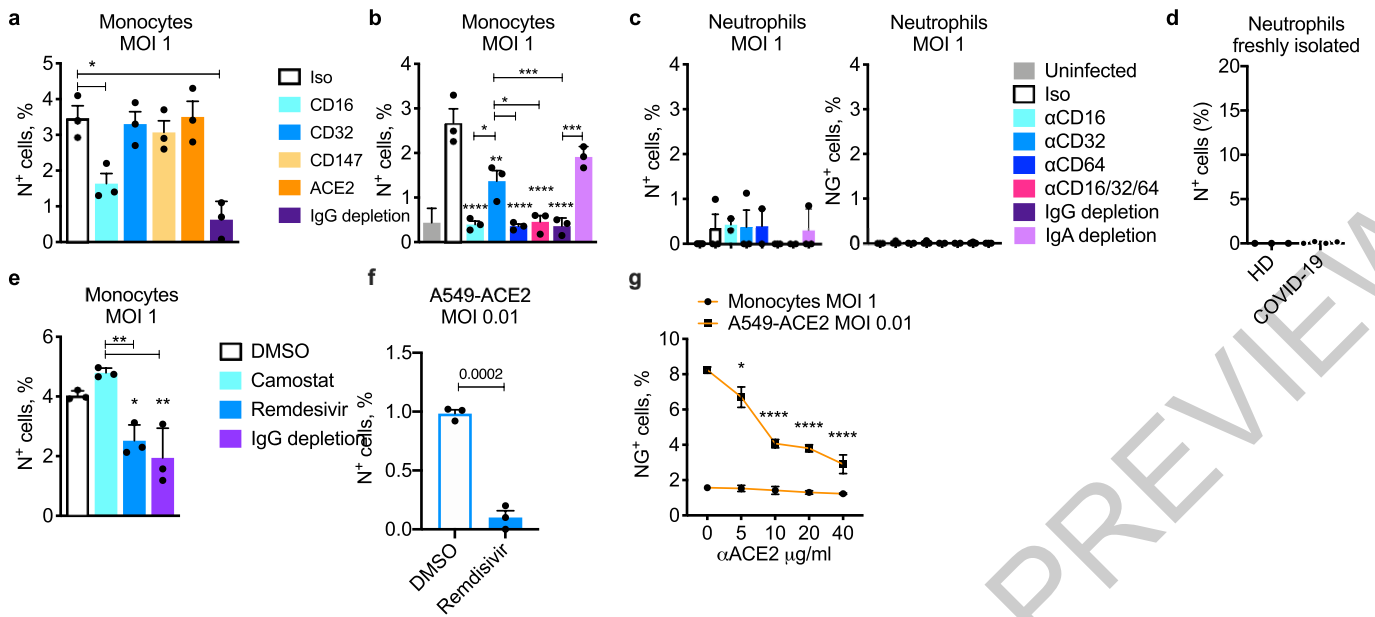
Extended Data Fig. 5 | In vitro infection of healthy donor monocytes and neutrophils. a-c, LPS-primed HD monocytes (n=3) (**a,b**) or purified HD neutrophils (n=3) (**c**) were infected with icSARS-CoV-2-mNG (MOI, 1), then stained 48 h later for nucleocapsid (N) or analyzed for NG fluorescence (**c**, right). Before infection, virus was preincubated with COVID-19 plasma, depleted or not of IgG as indicated, and infection was carried out in the presence of indicated blocking or isotype (Iso) control antibodies (**a-c**). The monocyte and neutrophil infections in (**b**) and (**c**) were performed with cells isolated from the same HDs. **d,** Freshly isolated neutrophils, enriched by negative selection, from HD (n=3) and COVID-19 patients of mixed disease severity (n=4) were stained for N and analyzed by flow cytometry to assess in vivo infection. **e,** Infection of LPS-primed HD monocytes (n=3) with icSARS-CoV-2-mNG in the presence of pooled COVID-19 patient plasma, depleted or not of IgG as indicated, and antiviral drugs, Camostat and Remdesivir. **f,** Infection of A549-ACE2 (n=3) with icSARS-CoV-2-mNG to verify the inhibitory activity of 10 μM Remdesivir. Infection was measured by N staining and flow cytometry. **g,** Infection of A549-ACE2 (n=3) and HD monocytes (n=3) with icSARS-CoV-2-mNG in the presence of anti-ACE2 blocking antibody at different concentrations. Infection was measured by NG fluorescence. Mean ± S.E.M. is shown. *p<0.05, **p<0.01, ***p<0.001, by one-way ANOVA with Tukey's multiple comparisons test (**a-c,g**), nonparametric unpaired *t*-test (**d,f**) and two-tailed nonparametric unpaired multiple *t*-test (**e**). Data are representative of 2 replicate experiments.

Corresponding author(s):	Judy Lieberman, MD, PhD
	Caroline Junqueira, PhD
Last updated by author(s):	Jan 24, 2021

Reporting Summary

Nature Research wishes to improve the reproducibility of the work that we publish. This form provides structure for consistency and transparency in reporting. For further information on Nature Research policies, see our Editorial Policies and the Editorial Policy Checklist.

Statistics

For all statistical analyses, confirm that the following items are present in the figure legend, table legend, main text, or Methods section.

n/a	Confirmed	
☐	☒	The exact sample size (n) for each experimental group/condition, given as a discrete number and unit of measurement
☐	☒	A statement on whether measurements were taken from distinct samples or whether the same sample was measured repeatedly
☐	☒	The statistical test(s) used AND whether they are one- or two-sided *Only common tests should be described solely by name; describe more complex techniques in the Methods section.*
☐	☒	A description of all covariates tested
☐	☒	A description of any assumptions or corrections, such as tests of normality and adjustment for multiple comparisons
☐	☒	A full description of the statistical parameters including central tendency (e.g. means) or other basic estimates (e.g. regression coefficient) AND variation (e.g. standard deviation) or associated estimates of uncertainty (e.g. confidence intervals)
☐	☒	For null hypothesis testing, the test statistic (e.g. F, t, r) with confidence intervals, effect sizes, degrees of freedom and P value noted *Give P values as exact values whenever suitable.*
☒	☐	For Bayesian analysis, information on the choice of priors and Markov chain Monte Carlo settings
☒	☐	For hierarchical and complex designs, identification of the appropriate level for tests and full reporting of outcomes
☐	☒	Estimates of effect sizes (e.g. Cohen's d, Pearson's r), indicating how they were calculated

Our web collection on statistics for biologists contains articles on many of the points above.

Software and code

Policy information about availability of computer code

Data collection	Flow cytometry data were acquired with FACSDiva v 7.0 (BD) Imaging Flow cytometry data were acquired with INSPIRE v 2 (Amnis - Millipore) GSDMD ELISA and LDH activity assay data were acquired with Gen5 (BioTek) Luminex Multiplex assay data were acquired with Luminex xPONENT 4.2 for MagPix Confocal microscopy images were acquired with Zen Black 2.0 (Zeiss) Pathology immunofluorescence slides were aquired with Aperio Versa console software v 1.0.4.125. qPCR data were acquired with BioRad CFX Manager Software v 1.6 IL-1b quantification by Ella was acquired with Simple Plex Runner 3.7.2.0
Data analysis	Flow cytometry data were analyzed with FlowJo v 10.7.1 (BD) Imaging Flow Cytometry data were analyzed with IDEAS v 6.2 (Amnis - Millipore) Luminex Multiplex assay data were analyzed with Milliplex Analyst v 5 (VigeneTech) Confocal microscopy images were processed with Zen Blue v 3.2 (Zeiss) qPCR data were analyzed with BioRad CFX Manager Software v 1.6 Pathology immunofluorescence slides were analyzed with Aperio ImageScope v 12.4.3 Graph design and statistical analysis were performed with GraphPad Prism v 9.0. IL-1b quantification by Ella was analyzed with Simple Plex Explorer 3.7.2.0

For manuscripts utilizing custom algorithms or software that are central to the research but not yet described in published literature, software must be made available to editors and reviewers. We strongly encourage code deposition in a community repository (e.g. GitHub). See the Nature Research guidelines for submitting code & software for further information.

Data

All manuscripts must include a data availability statement. This statement should provide the following information, where applicable:

- Accession codes, unique identifiers, or web links for publicly available datasets
- A list of figures that have associated raw data
- A description of any restrictions on data availability

SARS-CoV-2 isolated variants are available at MassCPR variant repository.
The minimum dataset necessary to interpret the findings are included in the article. Any further data that support the findings of this study are available from the corresponding authors upon request.

Field-specific reporting

Please select the one below that is the best fit for your research. If you are not sure, read the appropriate sections before making your selection.

☒ Life sciences   ☐ Behavioural & social sciences   ☐ Ecological, evolutionary & environmental sciences

For a reference copy of the document with all sections, see nature.com/documents/nr-reporting-summary-flat.pdf

Life sciences study design

All studies must disclose on these points even when the disclosure is negative.

Sample size	Our study enrolled 73 patients presenting at the Massachusetts General Hospital (MGH) emergency department (ED) (Boston, USA) with clinical symptoms suggestive of COVID-19, as well as 32 healthy donors (HD) over the course of 16 months. 5 of the MGH patients tested negative by qRT-PCR for SARS-CoV-2 and were included as non-COVID-19 samples. No methods were applied to calculate statistical power. 22 COVID patients and 19 HD were included in the freshly isolated phenotypic analysis presented in Figure 1a-b. 12 COVID patients and 10 HD were included in the ex vivo characterization of Figure 1c-e. 68 COVID patients, 5 non-COVID-19 and 20 HD were included in the plasma analysis presented in Figure 1f,g. For all other phenotypic characterizations by imaging flow cytometry, flow cytometry and qRT-PCR (Figures 2 and 3, Extended data Figure 2 and 3), the sample size had a minimum of 4 HD, non-COVID-19 and COVID-19 subjects. The number of subjects examined depended on the number of subjects available at each collection day and their cell yield. The in vitro infection assays (Figure 4 and Extended Data Figure 4 and 5) were performed with a minimum of 3 healthy donors (on the same day) whose blood was collected at Brigham and Women's Hospital Blood Bank. In addition, plasma from a separate cohort of 60 COVID-19 patients presenting to the MGH ED AND 10 HD was included in Figure 1f. No methods were applied to calculate statistical power. Plasma was collected on day 0 (n=60) and also on days 3 (n=42) and 7 (n=35) if the patients were hospitalized. Lung autopsies from 5 COVID-19 deceased patients and 3 trauma-related patient were used to quantify virus-infected cells and ASC speck formation.
Data exclusions	Previously vaccinated patients, who had breakthrough infections, were excluded from this manuscript to avoid confounding effects of vaccination on antibody-mediated infection. This was decided before the data analysis but not before sample collection.
Replication	Inflammasome detection experiments (Figure 2a-c) were performed at least 3 times with at least one HD and one COVID patient each time. The data presented combines all donors tested. In vitro infection assays (Figure 4 and Extended Data Figure 4 and 5) were performed at least 2 times with 3 donors at a time. No experimental data was excluded because of lack of reproducibility.
Randomization	The inclusion of patients in our study was completely random. Subjects were assigned as they arrived at the MGH ED if they agreed to consent. The Brigham and Women's Blood Bank provided random,unidentified healthy donor samples of materials that would have been discarded.
Blinding	All the data acquisition of plasma samples and flow cytometry and imaging flow cytometry acquisitions were performed blinded as to their SARS-CoV-2 infection status.

Reporting for specific materials, systems and methods

We require information from authors about some types of materials, experimental systems and methods used in many studies. Here, indicate whether each material, system or method listed is relevant to your study. If you are not sure if a list item applies to your research, read the appropriate section before selecting a response.

Materials & experimental systems

n/a	Involved in the study
☐	☒ Antibodies
☐	☒ Eukaryotic cell lines
☒	☐ Palaeontology and archaeology
☒	☐ Animals and other organisms
☐	☒ Human research participants
☒	☐ Clinical data
☒	☐ Dual use research of concern

Methods

n/a	Involved in the study
☒	☐ ChIP-seq
☐	☒ Flow cytometry
☒	☐ MRI-based neuroimaging

Antibodies

Antibodies used	Reagent or Resource Source Identifier (clone, Cat. #)

Antibodies
Flow Cytometry   Dilution
Mouse anti-human PerCP-Cy5.5 CD4 BioLegend Clone SK3; Cat. # 344608 1:200
Mouse anti-human PE-Cy7 CD14 BioLegend Clone HCD14; Cat. # 325618 1:200
Mouse anti-human PE CD16 BioLegend Clone 3G8; Cat. # 302008 1:200
Mouse anti-human APC CD16 BD Biosciences Clone B73.1; Cat. # 561304 1:200
Mouse anti-human PE-CF594 CD16 BD Biosciences Clone 3G8; Cat. # 562320 1:200
Mouse anti-human AlexaFluor 488 CD19 BioLegend Clone SJ25C1; Cat. # 363038 1:200
Mouse anti-human APC-Cy7 CD19 BioLegend Clone SJ25C1; Cat. # 363010 1:200
Mouse anti-human Brilliant Violet 650 CD19 BioLegend Clone HIB19; Cat. # 302237 1:100
Mouse anti-human APC-Cy7 CD8 BioLegend Clone SK1; Cat. # 344714 1:200
Mouse anti-human Brilliant Violet 421 CD3 BioLegend Clone UCHT1; Cat. # 300434 1:200
Mouse anti-human APC-Cy7 CD3 BioLegend Clone UCHT1; Cat. # 300426 1:200
Mouse anti-human APC-Cy7 CD56 BioLegend Clone HCD56; Cat. # 318332 1:100
Mouse anti-human Brilliant UltraViolet 737 CD56 BD Biosciences Clone NCAM16.2; Cat. # 349105 1:200
Mouse anti-human AlexaFluor 488 HLA-DR BioLegend Clone G46-6; Cat.# 307620 1:200
Mouse anti-human Brilliant UltraViolet 395 HLA-DR BD Biosciences Clone G46-6; Cat. # 564040 1:200
Mouse anti-human PerCP-Cy5.5 CD123 BD Biosciences Clone 7G3; Cat. # 558714 1:100
Mouse anti-human Brilliant Violet 421 CD11c BD Biosciences Clone B-LY6; Cat. # 562561 1:200
Mouse anti-human purified CD32 StemCell Technologies Clone IV.3; Cat. # 60012 1:100
Goat anti-human/mouse/rat/hamster purified ACE2 R&D Systems Polyclonal; Cat # AF933 1:100
Normal Goat IgG Control R&D Systems Polyclonal; Cat # AB108C 1:100
Mouse anti-human APC CD147 BioLegend Clone HIM6; Cat # 306214 1:100
Imaging Flow Cytometry, Immunofluorescence and Western blot
Mouse anti-dsRNA SCICONS Clone J2; Cat. # 1001020 1:500
Rabbit purified anti-SARS-CoV-2 Nucleocapsid GeneTex Polyclonal; Cat. # GTX135357 1:500
Mouse anti-human ASC Sigma Clone 2EI-7; Cat. # 04-147 1:200
Rabbit anti-human ASC Santa Cruz Polyclonal; Cat. # sc-22514-R 1:200
Goat anti-human NLRP3 Abcam Polyclonal; Cat. # ab4207 1:200
Mouse anti-human AIM2 Abcam Clone 3C4G11; Cat. # ab204995 1:200
Rabbit anti-human MEFV (Pyrin) Proteintech Polyclonal; Cat. # 24280-1-AP 1:200
Mouse anti-human GSDMD Lieberman lab Hybridoma (ref 55) 1:200
Rabbit anti-human GSDMD C-terminal Abcam Clone EPR19829; Cat. # ab210070 1:1000
Rabbit anti-human COX-IV Cell Signaling Clone 3E11; Cat. # 4850S 1:1000
Mouse anti-b-actin DSHB Polyclonal; Cat. # JLA-20 1:1000
Rabbit anti-SARS Nucleocapsid Novus Polyclonal; Cat. # NB100-56576 1:500
Rabbit anti-human CD14 Cell Signaling Clone D7A2T; Cat. # 75181 1:100
Rabbit anti-human CD31 Abcan Polyclonal; Cat. # ab28364 1:100
Mouse anti-human E-cadherin Santa Cruz Clone G-10; Cat. # sc-8426 1:100
Mouse anti-human ASC Santa Cruz Clone B-3; Cat. # sc-514414 1:100
Donkey anti-Rabbit IgG (H+L) Highly Cross-Adsorbed Secondary Antibody, Alexa Fluor 488 ThermoFisher Polyclonal; Cat. # A-21206 1:1000
Donkey anti-Rabbit IgG (H+L) Highly Cross-Adsorbed Secondary Antibody, Alexa Fluor 647 ThermoFisher Polyclonal; Cat. # A-31573 1:1000
Donkey anti-Mouse IgG (H+L) Highly Cross-Adsorbed Secondary Antibody, Alexa Fluor 647 ThermoFisher Polyclonal; Cat. # A-31571 1:1000
Donkey anti-Mouse IgG (H+L) Highly Cross-Adsorbed Secondary Antibody, Alexa Fluor 488 ThermoFisher Polyclonal; Cat. # A-21202 1:1000
Donkey anti-Goat IgG (H+L) Cross-Adsorbed Secondary Antibody, Alexa Fluor 568 ThermoFisher Polyclonal; Cat. # A-11057 1:1000
Donkey anti-Goat IgG (H+L) Cross-Adsorbed Secondary Antibody, Alexa Fluor 488 ThermoFisher Polyclonal; Cat. # A-11055 1:1000
Donkey anti-Goat IgG (H+L) Cross-Adsorbed Secondary Antibody, Alexa Fluor 647 ThermoFisher Polyclonal; Cat. # A-21447 1:1000
Amersham ECL Mouse IgG, HRP-linked whole Ab (from sheep) Cytiva Life sciences Polyclonal; Cat. # NA931-1ML 1:5000
Amersham ECL Rabbit IgG, HRP-linked whole Ab (from donkey) Cytiva Life sciences Polyclonal; Cat. # NA934-1ML 1:5000
Alexa Fluor 488 Tyramide ThermoFisher Cat. #B40953
Alexa Fluor 555 Tyramide ThermoFisher Cat. #B40955
Alexa Fluor 594 Tyramide ThermoFisher Cat. #B40957
Alexa Fluor 647 Tyramide ThermoFisher Cat. #B40958

Functional Assays
Human IgG1 Johnatan Abraham, Harvard Medical School Clone mAb114 10 µg/ml
Human anti-SARS-CoV-2 Spike protein, neutralizing Johnatan Abraham, Harvard Medical School Clone C1A-B12 10 µg/ml
Human anti-SARS-CoV-2 Spike protein, non-neutralizing Johnatan Abraham, Harvard Medical School Clone C1A-H12 10 µg/ml
Ultra-LEAF Purified anti-human CD16 Antibody BioLegend Clone 3G8; Cat. # 302050 10 µg/ml
Anti-human CD32 Monoclonal Antibody StemCell Technologies Clone IV.3; Cat. # 60012 10 µg/ml
Anti-human CD32 Monoclonal Antibody ThermoFisher Clone 6C4; Cat. # 16-0329-81 10 µg/ml
Ultra-LEAF Purified anti-human CD64 Antibody BioLegend Clone 10.1; Cat. # 305048 10 µg/ml
Ultra-LEAF Purified Mouse IgG1, κ Isotype Ctrl Antibody BioLegend Clone MOPC-21; Cat. # 400165 5-40 µg/ml
Goat anti-human/mouse/rat/hamster purified ACE2 R&D systems Polyclonal; Cat. # AF933 10 µg/ml
Normal Goat IgG Control R&D Systems Polyclonal; Cat. # AB108C 10 µg/ml
Ultra-LEAF Purified anti-human CD147 Antibody BioLegend Clone HIM6; Cat. # 306221 10 µg/ml

Validation | Each antibody and dye was validated following the manufacturer's instructions or based on previously published methods. The antibodies and dyes were titrated to obtain the optimal concentration for use in our panels. All primary antibodies were human-specific. The secondary antibody host species was chosen according to the primary antibody. The antibody specificity was compared to isotype control where applicable.

Eukaryotic cell lines

Policy information about cell lines

Cell line source(s) | THP-1 (ATCC), Vero-E6 (ATCC), HEK293T and A549 overexpressing ACE2 (HEK293T and A549 parental cell line was from ATCC and was lentivirally transduced with ACE2 gene in Anne Goldfeld's lab (Boston Children's Hospital).

Authentication | Cells were low passage cells from ATCC, which authenticates them. Cell morphology and growth was consistent with THP-1, and the cells showed signs of inflammasome activation once stimulated with the right reagents. ACE2 overexpression in HEK293T and A549 cells was confirmed by flow cytometry.

Mycoplasma contamination | Cells were frequently tested for mycoplasma contamination and were negative.

Commonly misidentified lines
(See ICLAC register) | None

Human research participants

Policy information about studies involving human research participants

Population characteristics | The fresh PBMC cohort were patients who enrolled in the MGH ED from 7/9/20 to 10/15/21. These included male and female patients 18 years or older (range 26-82) with clinical symptoms suggestive of COVID-19 infection (including one or more of the following: sore throat, congestion, cough, anosmia, shortness of breath, hypoxia, chest pain, fever, gastrointestinal symptoms, abdominal pain, nausea or vomiting and diarrhea). All patients testing positive by qRT-PCR for SARS-CoV-2 were included in the study, independently of race, ethnicity, BMI (range 18.00-47.81), co-morbidities, or whether they were receiving immunosuppressive treatment (3 patients). Blood was collected on the same day as the swab collection for PCR test. Clinical course was followed for 7 d post-enrollment or until hospital discharge, if that occurred after 7 d. Patients were assigned a maximum acuity score (A1-A5) based on their worst illness severity over 7 days (A1 – died (n=0), A2 – required mechanical ventilation (n=5), A3 – hospitalized requiring supplemental oxygen (n=18), A4 – hospitalized not requiring supplemental oxygen (n=4), A5 – discharged and not requiring subsequent hospitalization (n=4)).

The frozen plasma cohort included 60 patients who enrolled in the MGH ED from 3/15/20 to 4/15/20. These included patients 18 yr or older (range 20-80+) with clinical symptoms suggestive of COVID-19 infection and at least one of the following: (i) tachypnea ≥22 breaths per minute, (ii) oxygen saturation ≤92% on room air, (iii) requirement for supplemental oxygen, or (iv) positive-pressure ventilation. All patients testing positive by qRT-PCR for SARS-CoV-2 were included in the study, independently of race, ethnicity, BMI or co-morbidities. Blood was obtained at presentation, on the same day as the swab collection for PCR test (n=60) and on days 3 (n=42) and 7 (n=35) if the patient was hospitalized on those dates. Clinical course was followed for 28 d post-enrollment or until hospital discharge if after 28 d. SARS-CoV-2-confirmed patients (by qRT-PCR) were assigned a maximum acuity score (A1-A5) based on their worst illness severity over 28 d and were divided into three groups for comparison— severe (A1 – died, A2 – required mechanical ventilation, n=32), moderate (A3 – hospitalized requiring supplemental oxygen, n=16), and mild (A4 – hospitalized not requiring supplemental oxygen, A5 – discharged and not requiring subsequent hospitalization, n=12).

Lung autopsies cohort included 5 COVID-19 deceased patients and 3 trauma-related deceased patient and without lung disease. Lung specimens were obtained within 24 h of autopsy from Massachusetts General Hospital (MGH).

Anonymous healthy donor blood samples were obtained from the blood bank at Brigham and Women's Hospital in Boston, USA.

Recruitment | The fresh PBMC cohort was recruited by study coordinators from patients 18 years or older who were enrolled in the MGH ED from 7/9/20 to 10/15/21 with clinical symptoms suggestive of COVID-19 infection. All recruited patients provided signed informed consent. A 10-ml EDTA blood sample was transported to Boston Children's Hospital and processed within 2 h of collection. Only patients testing positive by qRT-PCR for SARS-CoV-2 were included in the study. The MGH COVID-19

Collection & Processing Team was in charge of recruitment.

The frozen plasma cohort included 60 patients that were enrolled in the MGH ED from 3/15/20 to 4/15/20 with an IRB-approved waiver of informed consent. These included patients 18 yr or older (range 20-80+) with clinical symptoms suggestive of COVID-19 infection and at least one of the following: (i) tachypnea ≥22 breaths per minute, (ii) oxygen saturation ≤92% on room air, (iii) requirement for supplemental oxygen, or (iv) positive-pressure ventilation. All patients testing positive by qRT-PCR for SARS-CoV-2 were included in the study. A 10-ml EDTA tube was obtained with the initial clinical blood draw in the ED (n=60) and on days 3 (n=42) and 7 (n=35) if the patient was hospitalized on those dates. Clinical course was followed for 28 d post-enrollment or until hospital discharge if after 28 d. The MGH COVID-19 Collection & Processing Team was in charge of recruitment.

Lung samples from 5 deceased individuals were obtained from Massachusetts General Hospital (MGH). Informed consent was obtained from relatives of study participants.

Anonymous healthy donor blood samples were obtained from the blood bank at Brigham and Women's Hospital in Boston, USA.

| Ethics oversight | Boston Children's Hospital and Massachusetts General Hospital Internal Review Boards |

Note that full information on the approval of the study protocol must also be provided in the manuscript.

Flow Cytometry

Plots

Confirm that:

☒ The axis labels state the marker and fluorochrome used (e.g. CD4-FITC).

☒ The axis scales are clearly visible. Include numbers along axes only for bottom left plot of group (a 'group' is an analysis of identical markers).

☒ All plots are contour plots with outliers or pseudocolor plots.

☒ A numerical value for number of cells or percentage (with statistics) is provided.

Methodology

| Sample preparation | COVID-19 and HD samples were processed using recommended safety precautions in a BSL-2+ facility. PBMC were purified using Ficoll gradient centrifugation and subjected to red blood cell lysis (if necessary) with Red Blood Cell Lysing Buffer Hybri-Max. One fraction of PBMC was stained for flow cytometry, while the remaining cells were used for monocyte or neutrophil purification by negative selection using magnetic beads. Purity was always greater than 95%.

PBMC were washed and stained for viability with Zombie Yellow in PBS (1:200) for 15 min on ice. Cells were washed with PBS, centrifuged, and then stained with Annexin V PE (1:200) in 1x Annexin Buffer for 15 min on ice. After washing with 1x Annexin V buffer, cells were blocked for 10 min with anti-CD32 (1:100) in PBS + 3% FBS. PBMC were then stained for 15 min on ice with a cocktail of antibodies to identify lymphocyte and myeloid cell subsets (all 1:200 except CD19 BV650, CD123 PerCP-Cy5.5 and CD56 APC-Cy7, 1:100). Purified monocytes were blocked with anti-CD32 and then stained with purified ACE2 antibody (1:100) for 15 min. The secondary anti-goat AF488 (1:1000) was coincubated with CD14 PE-Cy7 (1:200) and CD147 APC (1:100). After a last wash, PBMC or monocytes were resuspended in 2% PFA and kept at 4ºC until flow cytometry analysis.

Monocytes purified from HD PBMC using negative selection magnetic beads were cultured overnight in RPMI + 10% human AB serum and 1% Penicillin/Streptomycin with 100 ng/ml LPS. Monocytes or fresh isolated neutrophils were infected with icSARS-CoV-2-mNG (a molecular clone of SARS-CoV-2 expressing Neon Green fluorescent protein) using an MOI of 1 in a BSL-3 facility. The innoculum was treated with 10% COVID-19 patient pooled plasma (that had been depleted or not of IgG using Protein A/G agarose beads) before infection for 30 min at room temperature. 100 microliters of treated virus were added to monocytes (2x10^6 cells/well) in 48 well plates. Infected cells were incubated at 37ºC, 5% CO2 with gentle shaking every 10 min for 1 h, after which the culture volume was increased to 0.5 ml with RPMI supplemented with 5% heat inactivated normal AB human serum and 10% COVID-19 patient plasma (treated as described). Cultures were then incubated at 37ºC, 5% CO2 for 48 h at which time cells were harvested and fixed for 20 min with 4% PFA. Monocytes were then permeabilized with 0.1% Triton X-100, then blocked with PBS + 5% FBS. Cells were stained with primary antibodies for nucleocapsid (rabbit 1:500) then stained with secondary antibody (donkey anti-rabbit conjugated with AlexaFluor 647, at 1:1000) and anti-CD14 PE-Cy7. |

| Instrument | BD FACS Canto II and BD LSR II |

| Software | Flow cytometry data were acquired with FACSDiva (BD)
Flow cytometry data were analyzed with FlowJo v 10.7.1 (BD)
Graph design and statistical analysis were performed with GraphPad Prism V9.0. |

| Cell population abundance | All PBMC , all CD14+ monocytes or all neutrophils |

| Gating strategy | 1. PBMC and monocyte populations were identified by FSC-A/SSC-A.
2. PBMC and monocytes were gated as singlets by FSC-H/FSC-W. |

3. For assessment of cell death within PBMC (Figure 1a-c), specific cell populations were gated as shown in Extended Data Figure 1, and then Zombie/Annexin V percentages were analyzed.
4. For assessment of ACE2 and CD147 in HD and COVID-19 monocytes (Extended Data Figure 3) and J2/NeonGreen in SARS-CoV-2-infected HD monocytes (Figure 4, cells were gated in SSC-A/CD14+.

☒ Tick this box to confirm that a figure exemplifying the gating strategy is provided in the Supplementary Information.